Calhoun: The NPS Institutional Archive

DSpace Repository

Theses and Dissertations | 1. Thesis and Dissertation Collection, all items

2020-12

VISCOSITY MEASUREMENTS FOR INTERLAYER STRENGTH AND FAILURE IN ADDITIVELY MANUFACTURED PARTS

Tano, Mike

Monterey, CA; Naval Postgraduate School

http://hdl.handle.net/10945/66729

This publication is a work of the U.S. Government as defined in Title 17, United States Code, Section 101. Copyright protection is not available for this work in the United States.

Downloaded from NPS Archive: Calhoun

Calhoun is the Naval Postgraduate School's public access digital repository for research materials and institutional publications created by the NPS community. Calhoun is named for Professor of Mathematics Guy K. Calhoun, NPS's first appointed -- and published -- scholarly author.

Dudley Knox Library / Naval Postgraduate School
411 Dyer Road / 1 University Circle
Monterey, California USA 93943

http://www.nps.edu/library

NAVAL POSTGRADUATE SCHOOL

MONTEREY, CALIFORNIA

THESIS

VISCOSITY MEASUREMENTS FOR INTERLAYER STRENGTH AND FAILURE IN ADDITIVELY MANUFACTURED PARTS

by

Mike Tano

December 2020

Thesis Advisor: Ibrahim E. Gunduz
Second Reader: Jonathan Phillips

Approved for public release. Distribution is unlimited.

THIS PAGE INTENTIONALLY LEFT BLANK

REPORT DOCUMENTATION PAGE			Form Approved OMB No. 0704-0188

Public reporting burden for this collection of information is estimated to average 1 hour per response, including the time for reviewing instruction, searching existing data sources, gathering and maintaining the data needed, and completing and reviewing the collection of information. Send comments regarding this burden estimate or any other aspect of this collection of information, including suggestions for reducing this burden, to Washington headquarters Services, Directorate for Information Operations and Reports, 1215 Jefferson Davis Highway, Suite 1204, Arlington, VA 22202-4302, and to the Office of Management and Budget, Paperwork Reduction Project (0704-0188) Washington, DC, 20503.

1. AGENCY USE ONLY *(Leave blank)*	2. REPORT DATE December 2020	3. REPORT TYPE AND DATES COVERED Master's thesis

4. TITLE AND SUBTITLE VISCOSITY MEASUREMENTS FOR INTERLAYER STRENGTH AND FAILURE IN ADDITIVELY MANUFACTURED PARTS	5. FUNDING NUMBERS
6. AUTHOR(S) Mike Tano	
7. PERFORMING ORGANIZATION NAME(S) AND ADDRESS(ES) Naval Postgraduate School Monterey, CA 93943-5000	8. PERFORMING ORGANIZATION REPORT NUMBER
9. SPONSORING / MONITORING AGENCY NAME(S) AND ADDRESS(ES) N/A	10. SPONSORING / MONITORING AGENCY REPORT NUMBER

11. SUPPLEMENTARY NOTES The views expressed in this thesis are those of the author and do not reflect the official policy or position of the Department of Defense or the U.S. Government.

12a. DISTRIBUTION / AVAILABILITY STATEMENT Approved for public release. Distribution is unlimited.	12b. DISTRIBUTION CODE A

13. ABSTRACT (maximum 200 words)

Additive manufacturing (AM) holds considerable potential in the fabrication of multifunctional composites as well as printing components with optimized three-dimensional (3D) complex geometries layer by layer. However, the mechanical and thermal properties are not optimal for high precision and high performance applications. As the AM methods are transitioning from prototyping to fabrication, the interfaces between the precursor material properties, process parameters, structural resistance, and interlayer characteristics of 3D-printed parts are to be established. For AM applications using powder-based mixtures, it is necessary to understand the rheological properties of these non-Newtonian materials and their effects on deformation, stress, and viscosity, typically measured using a capillary rheometer. This research is focused on the viscosity of non-Newtonian heterogeneous polymer and powder mixtures used for direct-write AM using capillary rheometry and a custom measurement system for small-scale testing. This will help us understand the effects of deformation, stress, and viscosity to improve printed part properties such as interlayer strength.

14. SUBJECT TERMS additive manufacturing, viscosity, non-Newtonian polymer, 3D printing, capillary rheometry, direct-write AM, interlayer strength	15. NUMBER OF PAGES 73
	16. PRICE CODE

17. SECURITY CLASSIFICATION OF REPORT	18. SECURITY CLASSIFICATION OF THIS PAGE	19. SECURITY CLASSIFICATION OF ABSTRACT	20. LIMITATION OF ABSTRACT
Unclassified	Unclassified	Unclassified	UU

NSN 7540-01-280-5500

Standard Form 298 (Rev. 2-89)
Prescribed by ANSI Std. 239-18

THIS PAGE INTENTIONALLY LEFT BLANK

Approved for public release. Distribution is unlimited.

VISCOSITY MEASUREMENTS FOR INTERLAYER STRENGTH AND FAILURE IN ADDITIVELY MANUFACTURED PARTS

Mike Tano
Lieutenant Commander, United States Navy
BS, Embry-Riddle Aeronautical University, 2008

Submitted in partial fulfillment of the
requirements for the degree of

MASTER OF SCIENCE IN MECHANICAL ENGINEERING

from the

NAVAL POSTGRADUATE SCHOOL
December 2020

Approved by: Ibrahim E. Gunduz
Advisor

Jonathan Phillips
Second Reader

Garth V. Hobson
Chair, Department of Mechanical and Aerospace Engineering

THIS PAGE INTENTIONALLY LEFT BLANK

ABSTRACT

Additive manufacturing (AM) holds considerable potential in the fabrication of multifunctional composites as well as printing components with optimized three-dimensional (3D) complex geometries layer by layer. However, the mechanical and thermal properties are not optimal for high precision and high performance applications. As the AM methods are transitioning from prototyping to fabrication, the interfaces between the precursor material properties, process parameters, structural resistance, and interlayer characteristics of 3D-printed parts are to be established. For AM applications using powder-based mixtures, it is necessary to understand the rheological properties of these non-Newtonian materials and their effects on deformation, stress, and viscosity, typically measured using a capillary rheometer. This research is focused on the viscosity of non-Newtonian heterogeneous polymer and powder mixtures used for direct-write AM using capillary rheometry and a custom measurement system for small-scale testing. This will help us understand the effects of deformation, stress, and viscosity to improve printed part properties such as interlayer strength.

THIS PAGE INTENTIONALLY LEFT BLANK

TABLE OF CONTENTS

I. INTRODUCTION 1
- A. MOTIVATION 1
- B. BACKGROUND 5
  - 1. Additive Manufacturing 6
  - 2. Rheology of Non-Newtonian polymers 9
  - 3. Characterization of Additively Manufactured Products 17
- C. OBJECTIVE 21

II. EXPERIMENTAL MATERIALS AND METHODS 23
- A. MATERIALS 23
  - 1. Sculpey Oven Baked Clay 23
- B. EQUIPMENT 24
  - 1. Capillary Rheometer 24
  - 2. Mini Rheometer 25
- C. SAMPLE PREPARATION 27
  - 1. Sample Preparation 27
  - 2. Rosand RH2000 Capillary Rheometer 28
  - 3. Mini Rheometer V1 and V2 33

III. RESULTS AND DISCUSSION 37
- A. ROSAND RH2000 CAPILLARY RHEOMETER 37
- B. EMPIRICAL MODEL 42

IV. CONCLUSION 47

V. FUTURE WORK 49

LIST OF REFERENCES 51

INITIAL DISTRIBUTION LIST 55

THIS PAGE INTENTIONALLY LEFT BLANK

LIST OF FIGURES

Figure 1. Designs for mini rheometer (left) V1 and (right) V2. 4

Figure 2. Capillary rheometer twin bore system (Rosand RH2000). Source: [10]. 5

Figure 3. The first 3D printer invented by Charles Hull. Source: [13]. 6

Figure 4. Voxeljet VXC800. Source: [16]. 7

Figure 5. Materialise HeartPrint. Source [17]. 7

Figure 6. (A) Illustration of VAP process. (B) 3D system. Source: [19]. 8

Figure 7. Illustration of shear thinning and shear thickening behavior exhibited by non-Newtonian materials. Source: [22]. 10

Figure 8. Shearing surfaces for Poiseuille flow in a tube are cylinders sliding past one another. Source: [21]. 11

Figure 9. Geometry used in one type of commercial capillary rheometer. Source: [21]. 12

Figure 10. Example of a system undergoing shear flow (a) No slip (b) slip at the wall. Source [21]. 14

Figure 11. Schematic of how the derivative in WR correction is obtained from pressure drop and flow rate information. Source: [21]. 16

Figure 12. Schematic of the effect of material properties. Source: [21]. 16

Figure 13. Example of a pressure drop Versus L/R plot for polyethylene (PE). Source: [25]. 17

Figure 14. SEM TM 300 Hitachi High-Technologies Corporation. 19

Figure 15. Basic construction of a SEM. Source: [27]. 20

Figure 16. Energy Dispersive Spectroscopy (EDS) location. Source: [27]. 21

Figure 17. Example of an EDS spectrum. Source: [29]. 21

Figure 18. Sculpey oven-baked clay. Source: [31]. 23

Figure 19. Structure of polyvinyl chloride (PVC). Source: [32]. 23

Figure 20. Components of capillary rheometer (RH2000). Source: [34].....25

Figure 21. Mini rheometers V1 and V2 designs and 3D printed prototypes.....27

Figure 22. Sculpey clay sample.....27

Figure 23. (Left) Capillary rheometer (Rosand RH2000) (right) Installation of die.....28

Figure 24. Left and right bore die used for test#1.....31

Figure 25. Left and right bore die used for test#2.....31

Figure 26. Left and right bore die used for test#3.....31

Figure 27. Example of Mooney correction plot. Source [21].....33

Figure 28. 75-liter air compressor assisted with an air regulator used.....34

Figure 29. Measurements tool used.....35

Figure 30. Pressure drop (Dp) versus diameter plot for Sculpey clay.....37

Figure 31. Test#1 viscosity vs. shear rate plot.....38

Figure 32. Test#2 shear viscosity vs. shear rate plot.....39

Figure 33. Test#3 shear viscosity vs. shear rate plot.....41

Figure 34. Regression yield plot for each diameter.....42

Figure 35. Shear stress vs. shear rate for D = 0.5, 1 and 2 mm using HB model.....43

Figure 36. Apparent viscosity vs. shear rate for D = 0.5, 1 and 2 mm using HB model.....44

Figure 37. Mooney correction plot.....45

LIST OF TABLES

Table 1. Derivation of equations for Mooney, Bagley and WR correction. Adapted from [21].....13

Table 2. summary of the expressions for steady shear rheological quantities for common geometries. Adapted from [21]. 15

Table 3. Orifice diameter and length of dies.....29

Table 4. Die sizes used in testing for sample#1.....30

Table 5. Data for test#1(D=1mm).....38

Table 6. Data for test#2 (D=2mm).....39

Table 7. Data for test#3 (D=0.5mm).....40

THIS PAGE INTENTIONALLY LEFT BLANK

LIST OF ACRONYMS AND ABBREVIATIONS

3D	Three Dimensional
ABS	Acrylonitrile Butadiene Styrene
AM	Additive Manufacturing
ASTM	American Standard for Testing Materials
C	Carbon
Cl	Chloride
^{o}C	Celsius
DOD	Department of Department
DOE	Department of Energy
DSIAC	Department of Defense Systems Information Analysis Center
EDS	Energy-Dispersive X-ray Spectroscopy
FDM	Fused Deposition Modeling
HB	Herschel-Bulkley
ID	Inner Diameter
ISO	International Organization for Standardization
ISS	International Space Station
kN	Kilonewton
kPa	Kilopascal
L	Length
NDT	Non-Destructive Testing
PE	Polyethylene
PETG	Polyethylene terephthalate glycol
PLA	Polylactide
PVC	Polyvinyl chloride
OD	Outer Diameter
Q	Flow rate
R	Radius
R&D	Research and Development
SLA	Stereo Lithography
SEM	Scanning Electron Microscopy

TEM	Transmission Electron Microscopy
U.S.	United States
VAP	Vibrating Assisted Printing
WDS	Wavelength Dispersive Spectroscopy
XRD	X-ray Diffraction

ACKNOWLEDGMENTS

I would like to first and foremost give all honor, glory, eternal praise and thanks to God Elohim—our Heavenly Father and Heavenly Mother—for Their boundless love, patience and grace through this process.

I would like to thank my family and my parents, especially to my wife and my sons, for their prayers and endless support.

I would like to also thank Dr. Gunduz for his guidance, well-versed advice, and support throughout my thesis project. I would also like the thank Dr. Phillips for his keen advice.

Thank you to all my professors who offered me an amazing education and challenged me to go above and beyond. Thanks to my colleagues and military comrades Kaitlyn, Casie and Shawn for enduring together and sharing these amazing moments. Thank you to all the ME/MAE faculty and staff, especially CDR Arledge and Susan Lichtenwalter for always being there to listen, give keen advice and provide the necessary educational and professional support.

THIS PAGE INTENTIONALLY LEFT BLANK

I. INTRODUCTION

A. MOTIVATION

Additive manufacturing (AM) holds considerable potential in the fabrication of multifunctional composites, as well as printing components with optimized 3D complex geometries layer by layer at low manufacturing costs and/or reduced weight. AM can be considered a “clean agile manufacturing” method, as it minimizes environmental impact of manufacturing, and provides rapid and flexible fabrication paradigms [1]. AM has significantly advanced throughout the years and has renovated manufacturing and logistics processes by making them easier, faster, highly technical and highly specific. AM implementations include aerospace, energetics, military, and biomedical applications. The acceptance of AM in the military, in particular, was sought due to the advantages such as onsite manufacturing and production, less waste, and freedom of design and automation over traditional machining. In order to advance research and development (R&D) and procure great quantities of the type of components through AM, many interested federal agencies are establishing policies to support AM. For instance, to continue to maintain and enhance space dominance, NASA is currently conducting R&D into new materials and tools using AM, with the intent to promote its adequacy into space and space stations such as the international space station (ISS) [2].

Early defect detection and correction measures in 3D printing can help prevent reprinting objects for more advanced materials due to small errors [3]. Thermoplastic polymers including, but limited to, polylactide (PLA), nylon, polyethylene terephthalate glycol-modified (PETG), polyethylene (PE), polyvinyl chloride (PVC) are being utilized to manufacture precise and adaptable 3D complex geometry parts at reduced weight and low cost [4]. These can be mixed with other additive materials such as calcium carbonate and silica in order to improve their properties and the scope of 3D modelling process.

As an imminent technology, AM is widely pursued to support major and critical military and civilian applications. Scott et al. stated that Air Force and Navy are concurrently conducting research to instate AM into manufacturing of critical and non-

critical parts such as metal and thermoplastic composite parts for their fleet of aircrafts, autonomous and unmanned systems and ships; and also, to promptly certify AM parts to mitigate obsolescence of parts and to reduce procurement times [2]. For material extrusion type AM, the deformation or flow behaviors that occur during mixing, extrusion and other manufacturing processes are paramount in improving the AM system efficiency, quality of the end product and mitigating inconsistency [5].

There is tremendous need to improve and expand AM capabilities, technologies and interdisciplinary research programs, innovation and support. According to the Department of Defense Systems Information Analysis Center (DSIAC), the Department of Defense (DOD) is making systematic progress by implementing policies and plans to support its services with a federally-funded research programs and AM efforts including manufacturing critical and noncritical aircrafts, ships and submarines repair parts [6]. The investment into AM is expected to be substantial and for two consecutive year, AM growth rate in aerospace and medical fields was estimated at 25.9% with a U.S. capital growth of $1 billion [5]. The DOD budget allocated for 2018 was estimated to about $640 billion, with $13 billion set for AM technology innovation such as new types and designs of 3D printers of materials used in AM [7].

Significant concerns still exist despite all AM technology progresses made in several different applications, especially in aerospace and in defense space where quality assurance and control remain a key issue. As some AM processes involves the use of a thermal energy source for multiple layer fusion, different regions of the 3D printed parts experience repeated heating and cooling; thus, causing material mechanical and thermal properties defects to occur [8]. The structural defects (e.g., high porosity), unsatisfactory sealing properties, and other part failures can occur during the manufacturing process from the intense temperature gradients that take place during inter-layer welding [8]. As a result, the mechanical and thermal properties become inadequate for high-precision and high-performance applications. Solving these issues will allow AM to have the quality assurance needed to utilize the method for critical components, such as rocket nozzles for spacecraft or 3D-printed titanium links and fittings inside an engine of a MV-22 Osprey naval aircraft [9].

For AM applications using powder-based mixtures, it is necessary to understand the rheological properties of these non-Newtonian materials and its effects on deformation, stress, and viscosity, typically measured using a capillary rheometer. It would be value added to incorporate processes to control rheological properties of the materials during manufacturing process, permitting defect detection during production. The defects to be detected are those not only associated with immediate failure but also failures caused by life cycle and operational stresses of the parts [9].

This research is focused on the viscosity of non-Newtonian heterogeneous polymer and powder mixtures used for direct-write AM using capillary rheometry and a custom measurement system for small scale testing. This will help us understand the effects of deformation, stress, and viscosity to improve printed part properties such as interlayer strength. For this study, a capillary rheometer design called “mini rheometer” and an actual capillary rheometer RH 2000 twin bore system will be utilized. In mini rheometer, a prototype with a unique design and method of measurement system, the material will travel through a series of cylindrical reservoirs of various sizes, and carefully measure the pressure gradient across each cylindrical reservoir to a final extruded material. The extruded materials are those suitable for 3D printing. In RH 2000, the flow patterns, measurement of pressure and shear rate of extrusion of viscous and heterogeneous materials will be studied. It will also be used when high shear rates are required.

Figure 1 illustrates the mini rheometer V1 and V2, prototypes not yet tested, for small scale testing that is reflective of extrusion conditions during AM.

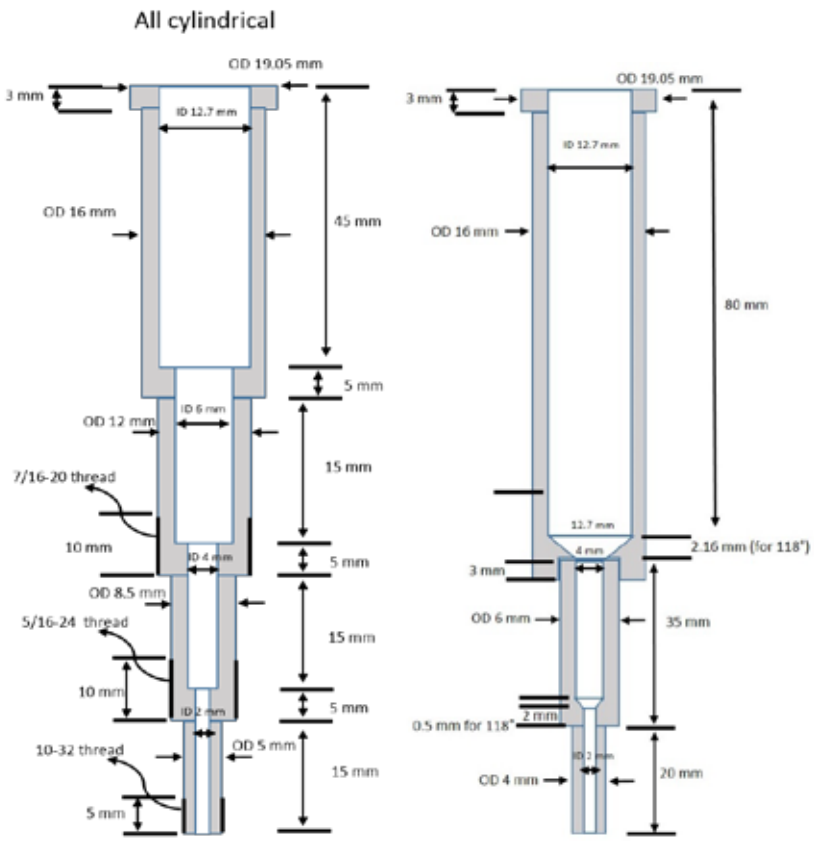

Figure 1. Designs for mini rheometer (left) V1 and (right) V2.

Figure 2 illustrates a capillary rheometer twin bore system that will be used to measure shear viscosity of the material flowing from the reservoir of the capillary rheometer into a die. This is with the intent to optimize material properties to minimize defect formation.

Figure 2. Capillary rheometer twin bore system (Rosand RH2000). Source: [10].

B. BACKGROUND

As the AM methods are transitioning from prototyping to fabrication, there is the need to consider the effect of material formulations on defect formation. It is assumed during AM process that all manufactured materials contained defects, these expected defects in the materials do not make the part inadequate for suitable applications and the detection of these defects increases as the size of the defects increases [11]. These defects can originate due to AM material formulations, can be managed by controlling the viscosity (which is temperature sensitive) of the materials. In other words, the materials have to be optimized to have the lowest viscosities possible for a given density.

The following sections provide the relevant background for AM, Rheology of non-Newtonian polymers and the relevant characterization methods that can be used to evaluate the properties, and performance of the processed materials.

1. Additive Manufacturing

International Organization for Standardization (ISO) and American Standard for Testing Materials (ASTM) defined AM as “the process of joining materials to make objects from 3-D model data, usually layer upon layer, as opposed to subtractive manufacturing technologies” [12]. AM is an innovative technique for manufacturing 3D complex structure and flexible geometries by “addition” of materials together. In the mid-1980s, this printing technique was popularized by Charles Hull, who introduced Stereo Lithography (SLA) (i.e., early 3D printing stage), which led to the innovation of other techniques including, but not limited to, powder bed fusion and fused deposition modelling (FDM), although a lot of the initial developments goes back to the late 1950s. Figure 3 illustrates the first 3D printer, invented by Charles Hull.

Figure 3. The first 3D printer, invented by Charles Hull. Source: [13].

Major different industries sought AM very early first for its rapid prototyping and later for its advantages such as onsite manufacturing and production, freedom of design and automation, over traditional machining. The current range of AM applications is extensive, ranging from medical treatment and mold design to automotive, and aeronautics for final net shape parts. Despite its benefits, there was little interest by the military in AM due to the initial high cost and uncertainties in material properties [14]. However, as the computer and processors continue to evolve in speed and accuracy, and

the cost of components such as stepper motors and drivers decrease, AM technologies are proportionally advancing and evolving; thus, improving material quality and lowering manufacturing cost [15]. Most recent 3D printing technologies, such as VX800 released by Voxeljet, which prints on an angled build plane that moves a conveyor, allows for unlimited lengths and continuous operation. Figure 4 illustrates Voxeljet VXC800. Also, HeartPrint from Materialise with patient-specific cardiovascular models for pre-surgery planning and device testing, have revolutionized the industry. Figure 5 illustrates Materialise HeartPrint.

Figure 4. Voxeljet VXC800. Source: [16].

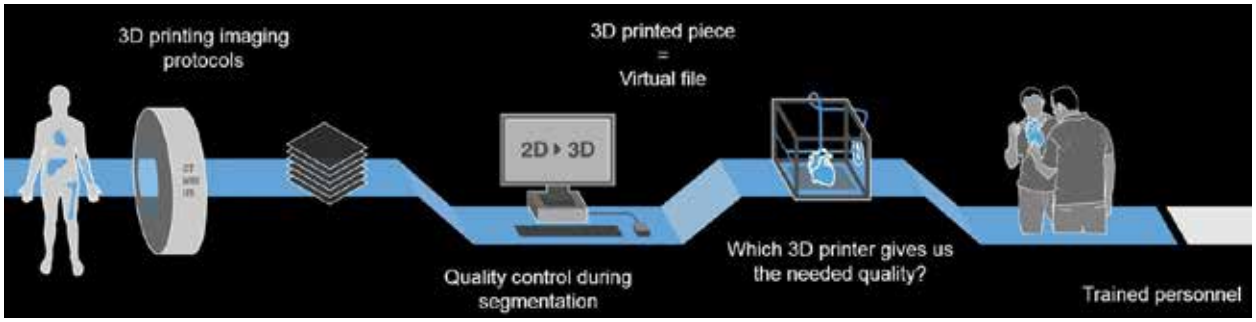

Figure 5. Materialise HeartPrint. Source [17].

A newer AM approach called Vibration Assisted Printing (VAP) provides a potential for creating composites at high resolution and with low porosity [18], [19]. Figure 6 illustrates the vibration Assisted Printing process. Gunduz et al. explained this direct-write approach resonates the print nozzle to increase vibration amplitudes. The vibrations assist flow by reducing the effective friction at the nozzle exit, allowing extremely viscous materials to be 3D-printed with lower porosity [19]. With the ability to drastically reduce the friction, VAP allows different higher-performance materials to be used that could not be previously processed due to their viscosity, while allowing better dimensional control of the part being printed.

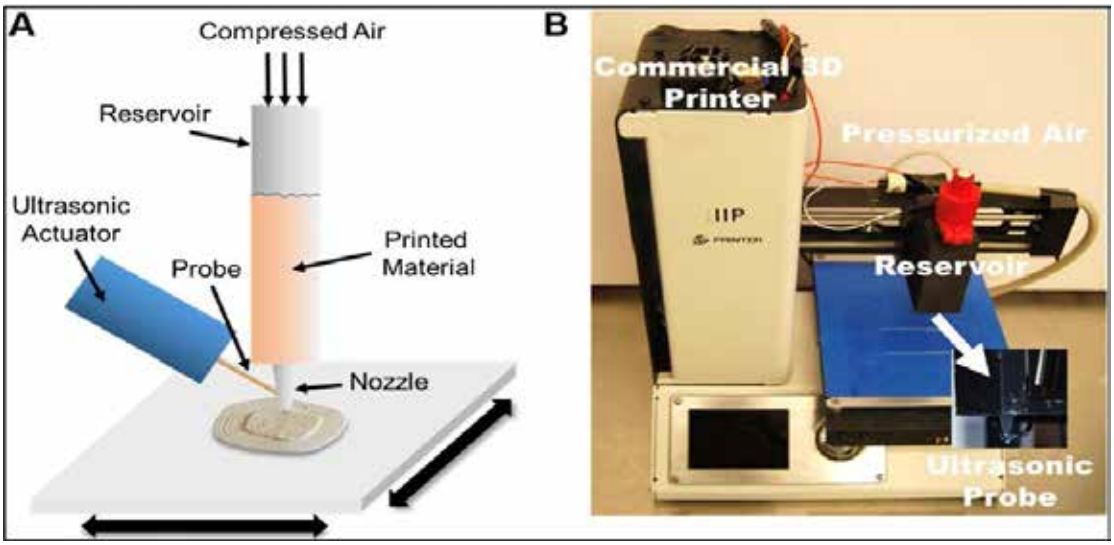

Figure 6. (A) Illustration of VAP process. (B) 3D system. Source: [19].

Gunduz et al. asserted VAP can process very high solids-loaded, (>80 wt.%) extremely viscous and low porosity powder-polymer mixtures at high resolutions and speeds [19], [20]. This new approach opens the way to unique AM advances. For example, the ability to print mixtures consisting mostly of different powders with small amounts variety of polymers, can result in high energy density energetics and sintered products coming out near net-shape with unique geometric features like cooling channels and potentially improved mechanical and thermal properties. Gunduz et al. determined since VAP AM can print more highly viscous materials and a better variety of materials,

the mixing methods and formulation optimization prior to 3D printing needs to be experimented on by varying weight percentages of components and rheological processing conditions [19], [20].

2. Rheology of Non-Newtonian polymers

Rheology is an important disciplinary field which deals with the deformation or flow behaviors of materials and stresses, and includes polymers, suspensions and inks, and plastic heterogenous solid mixtures [21]. The Rheology of polymers and pastes is used to determine the deformation and flow conditions required during processing, including AM processing, to assure the final parts made of these types of materials are of high quality.

The rheological properties of complex materials show a variety of behaviors such as non-Newtonian flow and shear thinning. Understanding the rheological properties of materials employed in AM, as well as continuous monitoring of these properties during processing can lead to appropriate manufacturing design, and on-line adjustments, leading to high quality parts, and reduction of waste [22]. Significant factors are required in the adequacy of rheology of a polymer. These factors include, but not limited to, polymer type, viscosity, stress, temperature, and shear rate. The rheology test capabilities can be applied in optimization of the measurable data to improve mechanical and thermal parameters; thus, leading to cost saving, less waste and even increase manufacturing rates. Information generated from rheology can ascertain mechanical and thermal properties of the polymer specifications and characterization are met and achieved respectively. Non-Newtonian polymers including, but not limited to PVC and PE, are a very interesting group of materials to study because the magnitude flow time constants and processing times are the identical. Therefore, it is paramount to control the deformation and flow of non-Newtonian polymers. The objective is to alter their structure so that the mechanical and thermal property of these materials can significantly improve without sacrificing the quality of the final product.

Moreover, to analyze and measure the rheological material properties, capillary rheometry and capillary rheometers, respectively, are sought. Capillary rheometry is very

useful tool for determining shear viscosity and flow properties of materials containing large particles, at high shear rate and applied force [23]. It is often used as a method to determine and analyze stress, shear rate, viscosity, ratio of shear stress and velocity gradient. Non-Newtonian material viscosity changes with shear rate. The non-ideal behaviors in non-Newtonian materials are shear thinning, where material becomes softer under higher stresses, but recovers when shear is removed, and shear thickening where material becomes stiff under stress, but softens when shear is removed. Shear thinning occurs because of rearrangements in the materials particles and microstructure in the planar direction of the applied shear [23]. Figure 7 illustrates shear thinning and shear thickening behavior exhibited by non-Newtonian materials.

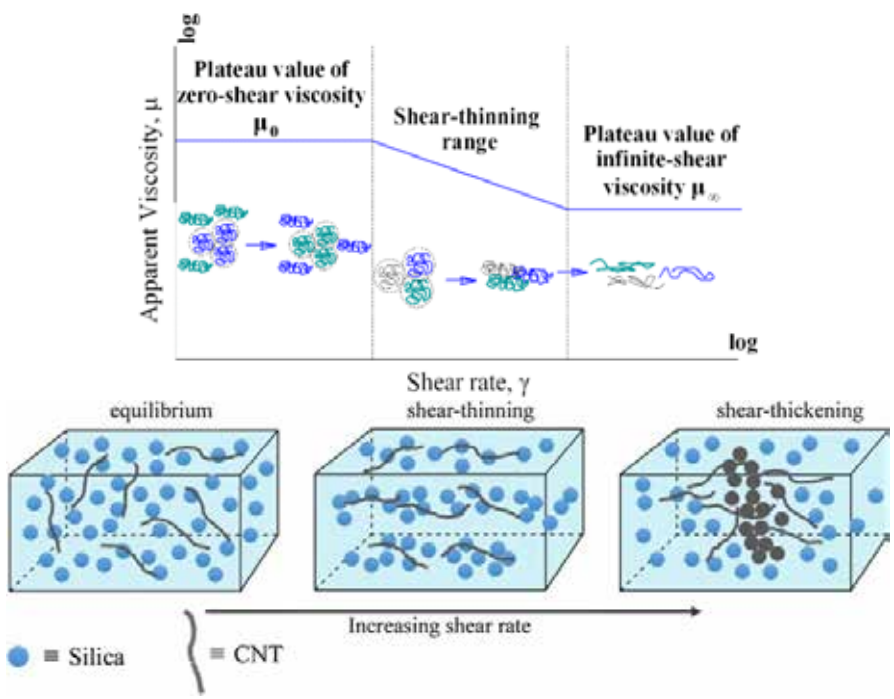

Figure 7. Illustration of shear thinning and shear thickening behavior exhibited by non-Newtonian materials. Source: [22].

Non-Newtonian materials can be utilized for AM, but they can be highly viscous initially and hard to extrude. Shear-thinning materials can flow through narrow nozzles and then freeze in place, which has been utilized in certain implementations of AM.

To study the rheological properties or behavior of materials under extrusion, capillary rheometers are used as an analysis technique for high viscosity materials. They help quantify and characterize the behavior of materials in response to particular forces or stresses. An applied force enables the investigation of behavior and quantify the viscosity, shear stress and shear rate [21]. In the capillary rheometer, the material flows through a narrow section called capillary. The flow through a capillary is considered unidirectional flow in which cylindrical surfaces slide past each other, called Poiseuille flow [21]. The material being tested resides in the upstream reservoir. Figure 8 illustrates shearing surfaces for Poiseuille flow in a tube are cylinders sliding past one another.

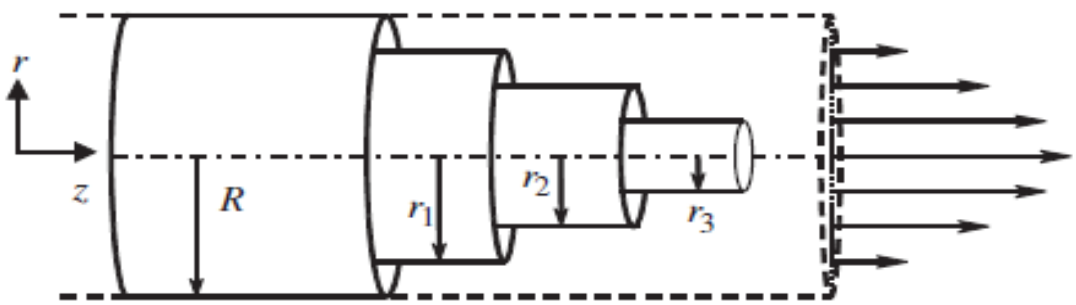

Figure 8. Shearing surfaces for Poiseuille flow in a tube are cylinders sliding past one another. Source: [21].

A piston pushes the material through a small capillary of radius (R), and the material exits at the bottom at a flow rate (Q). Many materials also exhibit die swell at high shear rates, a phenomenon where the diameter of the exiting fluid can be several times the diameter of the capillary from which it is flowing [21]. Figure 9 illustrates geometry used in one type of commercial capillary rheometer. The flow rate data and calculate shear viscosity of the material, the pressure drop (ΔP) across the barrel or die has to be measured under controlled shear rate and temperature [21].

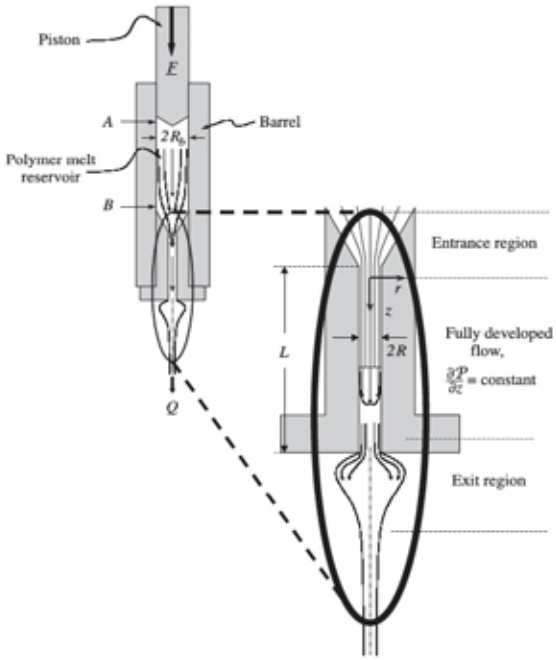

Figure 9. Geometry used in one type of commercial capillary rheometer. Source: [21].

Capillary rheometry is typically utilized to quantify viscosities very accurately at high applied forces and shear rates used in polymer processing by taking into account end effects and slip effects [21].

Due to deficiencies of capillary rheometers such as inconsistency of shear rate and erratic behavior at the entrance and exit to the capillary exhibited by materials, capillary flow corrections for non-Newtonian polymer are required [24]. In this regard, the following corrections are used: Mooney correction for wall slip correction, Bagley correction for entrance-pressure correction, and Weissenberg-Rabinowitsch (WR) correction for non-Newtonian fluid/non-parabolic velocity profile correction [21]. To support the corrections aforementioned and measurement of the behavior of a continuum of non-Newtonian polymers to external forces, the following equations are used: the equation of motion (i.e., momentum conservation), the continuity equation (i.e., mass conservation), and the constitutive equation that is a material-specific equation that indicates how deformation and stress are related. Table 1 illustrates these equations that are all the relations needed to solve flow problems. The corrections (i.e., Mooney, WR

and Bagley) involve derivation of equations in relation to flow rate (Q), shear stress (t), shear rate (g) and viscosity (m) taking into account wall slip, which is usually ignored.

Table 1. Derivation of equations for Mooney, Bagley and WR correction. Adapted from [21].

Shear stress equation (1)	$\tau_R = \frac{(P_0 - P_L)R}{2L}$ = ΔpR/2L
Mooney correction equation (2)	$\dot{\gamma}_a = \frac{4Q}{\pi R^3} = \frac{1}{\mu}\frac{\Delta PR}{2L} = \frac{4v_{z,av}}{R}$ $\dot{\gamma}_{a,slipcor} = \frac{4v_{z,av}}{R} - \frac{4v_{z,slip}}{R}$
WR correction equation (3)	$\dot{\gamma}_R = \dot{\gamma}_a \left[\frac{1}{4}\left(3 + \frac{dln\dot{\gamma}_a}{dln\tau_R}\right)\right]$
Bagley correction equation (4)	$\Delta p = 2\tau L/R$
Viscosity equation (5)	$\frac{(\mathcal{P}_0 - \mathcal{P}_L)R}{2L}\left(\frac{\pi R^3}{4Q}\right) = \mu$
Flow rate equation (6)	$Q = v\pi R^2$

The Mooney correction is needed to correct for wall slip that occurs which reduces the actual shear rate [21]. Figure 10 illustrates different velocity profile for no slip and slip at the wall. The effect of slip is to reduce the deformation experienced by the fluid. In the case where slip is occurring, as compared to the no-slip case, the shear rate is reduced throughout, but especially near the wall. The shear stress at the wall, τ_R, remains unaffected by the change in boundary condition. Important steps are required in order to perform the corrections: correct the apparent shear rate $\dot{\gamma}_a$ for slip using the no slip equation (2), rearrange shear rate $\dot{\gamma}_a$ (no slip) to obtain shear rate slip correction $\dot{\gamma}_{a,slipcor}$ ($table$ 1) and finally interpolate on the lines of pressure drop (Δp) versus flow

rate (Q) to obtain equal data points to shear stress at wall [21]. Figure 10 illustrates an example of a system undergoing shear flow no slip and slip at the wall.

The correction of the flow rate is achieved once slip velocities is tabulated. To calculate a viscosity in a situation where slip is occurring, the true shear rate near the wall must be calculated [21]. Tables 1and 2 illustrate the equations needed for the different corrections.

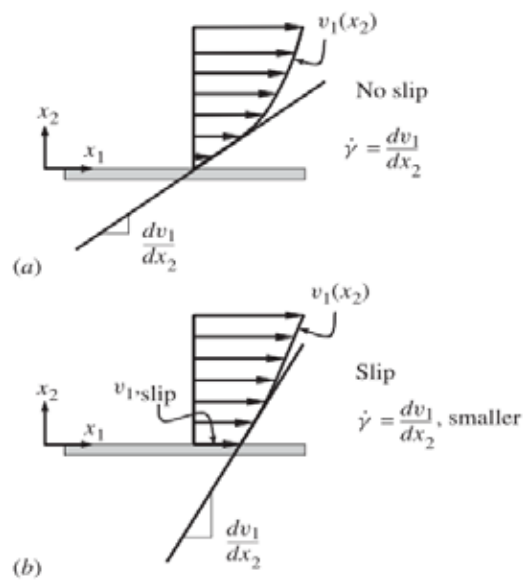

Figure 10. Example of a system undergoing shear flow (a) No slip (b) slip at the wall. Source [21].

The WR correction, for non-Newtonian fluids, uses the equation (3) in Table 1 to correct the wall shear rate. A no-slip condition was assumed at the capillary wall in the WR correction. The shear rate of the polymer is instable across capillary. Since the velocity varies at the wall and the difference between the true shear rate and the apparent shear is rectified by WR correction, non-Newtonian materials show greater change in velocity at the wall than Newtonian materials [24]. The true shear rate ($\dot{\gamma}_R$) can be calculated from equation (3) in Table 1. To calculate the WR from data, a plot ln $\dot{\gamma}_a$ versus ln τ_R is made (Figure 11). The WR correction also uses mathematical methods

depending of the shape of the line; a regression yields for straight line and polynomial for skew line from which the derivative can be obtained [21]. It can be tabulated and applied using the data point. The viscosity is the ratio of the shear stress and true shear rate at the wall [21]. It also accounts for the differences in shear rates between Newtonian polymers and the velocity profiles (i.e., non-parabolic) for non-Newtonian polymers. Figure 11 illustrates how the derivative in WR correction is obtained from pressure drop and flow rate information. Figure 12 describes shear thinning behavior for Newtonian and non-Newtonian fluid.

Table 2. Summary of the expressions for steady shear rheological quantities for common geometries. Adapted from [21].

Geometry	Magnitude of Shear Stress $\lvert\tau_{21}\rvert$	Shear Rate $\dot{\gamma}$	Measured Material Function
Capillary flow (wall conditions) $\mathcal{P}_0, \mathcal{P}_L$ = modified pressure at $z = 0, L$ Q = flow rate L = capillary length $\mathcal{R} = \frac{1}{4}\left[3 + \frac{d\ \ln(4Q/\pi R^3)}{d\ \ln \tau_R}\right]$ $\tau_R = \tau_{rz}\lvert_{r=R}$	$\frac{(\mathcal{P}_0 - \mathcal{P}_L)R}{2L}$	$\frac{4Q}{\pi R^3}\mathcal{R}$	$\eta = \frac{\tau_R}{4Q/\pi R^3}\mathcal{R}^{-1}$

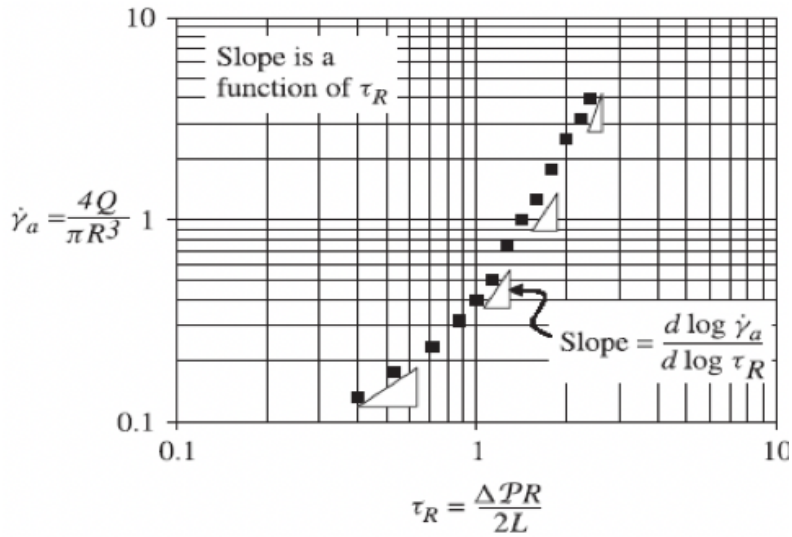

Figure 11. Schematic of how the derivative in WR correction is obtained from pressure drop and flow rate information. Source: [21].

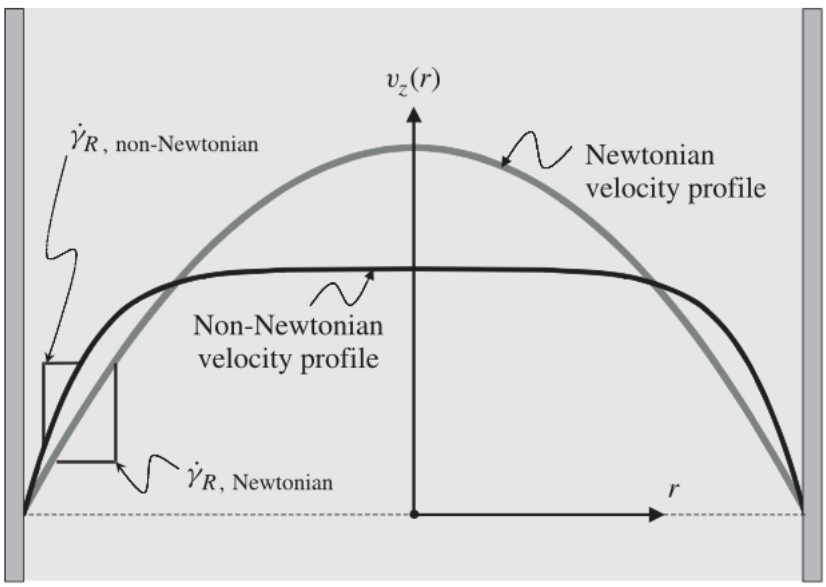

Figure 12. Schematic of the effect of material properties. Source: [21].

The Bagley correction correlates the entrance and exit effects of the orifice die. According to G. McNally et al., it corrects for pressure change at equilibrium due to die length differences. Bagley correction measures the flow rate data of the materials using ratios of at least two die of different length (L) and radius (R) [24]. At least two measured

shear rates are logged and ΔP versus L/R for different shear rates is plotted; then use the extrapolation of the lines at $\Delta P = 0$ to find the entry loss correction factor for each shear rate [24]. Figure 13 shows an example of a pressure drop Versus L/R plot for polyethylene (PE). E. Bagley asserted the correction for end effects at each apparent shear rate may be calculated either from the y-intercept or from the extrapolated x-intercept e [25].

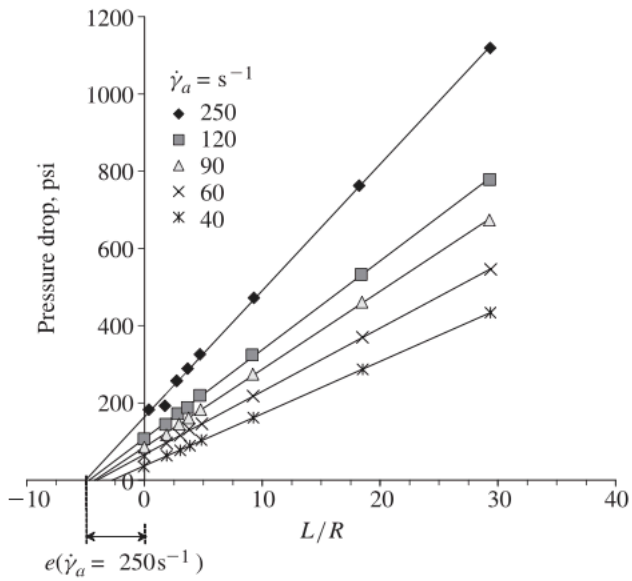

Figure 13. Example of a pressure drop Versus L/R plot for polyethylene (PE). Source: [25].

3. Characterization of Additively Manufactured Products

To enable the application of AM in major industries and composites, it is necessary to evaluate and analyze the microstructural features of AM parts in order to understand their mechanical and thermal properties. It is also important to identify characteristics of the components and/or elements that were utilized and the performance of the 3D printed parts. The relevant advanced characterization techniques include, but are not limited to, mechanical tensile and compression testing, microscopic imaging using a Scanning Electron Microscope (SEM), Energy-Dispersive X-ray Spectroscopy (EDS), Wavelength Dispersive Spectroscopy (WDS), X-ray Diffraction (XRD), Raman

Spectroscopy and Transmission Electron Microscopy (TEM). These techniques help in understanding the electron-specimen interactions more efficiently and enable more logical interpretation of the data or imagery collected, and thereby produce high quality results that can be utilized with rigor and confidence. The ASTM qualifies these techniques mentioned above as essential in quantifying the elemental composition of phases in microstructure and determining microstructure, porosity and composition of the materials that can influence their mechanical and thermal properties [26]. These techniques are valuable to conduct testing on materials to determine their microstructural properties and whether or not their performance and strength will meet the desired objective or mission. These techniques are critical in evaluating AM printed parts quality.

a. Scanning Electron Microscopy (SEM)

SEM is a scientific instrument that employs a rastering electron beam to form a high-resolution, black and white 3D images of an object and examine it on a very fine scale, thus making it possible to discover tiny defects and trace impurities that cause parts to corrode or break over time. SEM detects, analyzes and even examines surface and subsurface fractures and contaminations, and provide crystalline structures and chemical compositions information [27]. SEM's 3D images also provide information including, but not limited to, topography, morphology, and composition of the surface or subsurface of the sample which are vital for analysis. The analysis can be critical in determining the property characteristics and quality of the AM material. Figure 14 illustrates an image of SEM TM 300 Hitachi High-Technologies Corporation. Figure 15 illustrates Basic construction of a SEM.

Figure 14. SEM TM 300 Hitachi High-Technologies Corporation.

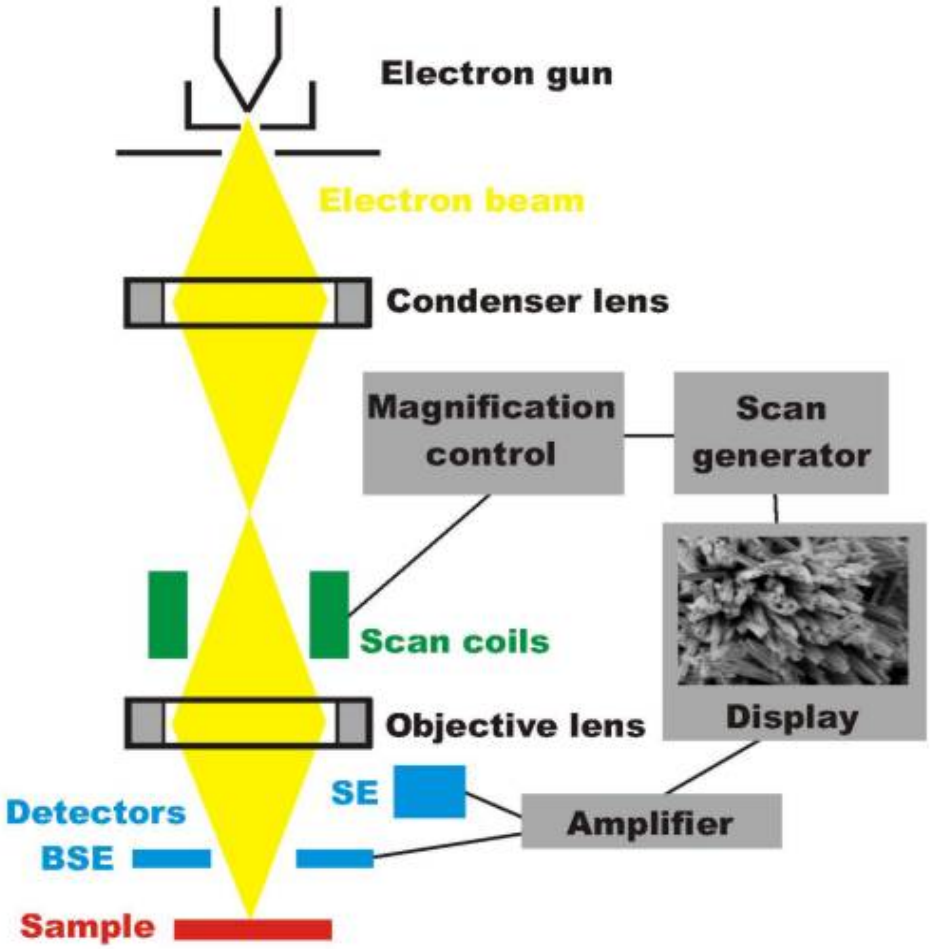

Figure 15. Basic construction of a SEM. Source: [27].

b. Energy Dispersive X-RAY Spectroscopy (EDS)

EDS, an analytical technique, that is often paired with SEM. It dissects the elemental composition and/or characterization of the sample [28]. During bombardment, electrons are ejected from the surface of the sample and EDS detects X-rays emitted from the sample. A higher state electron filled the empty space, and an energy balance occurs [28]. The X-ray energy emitted from the sample is specific to an elemental composition. Thus, the X-ray emitted provides essentially elemental composition of the sample.

Figure 16 illustrates EDS location and Figure 17 illustrates the EDS spectrum.

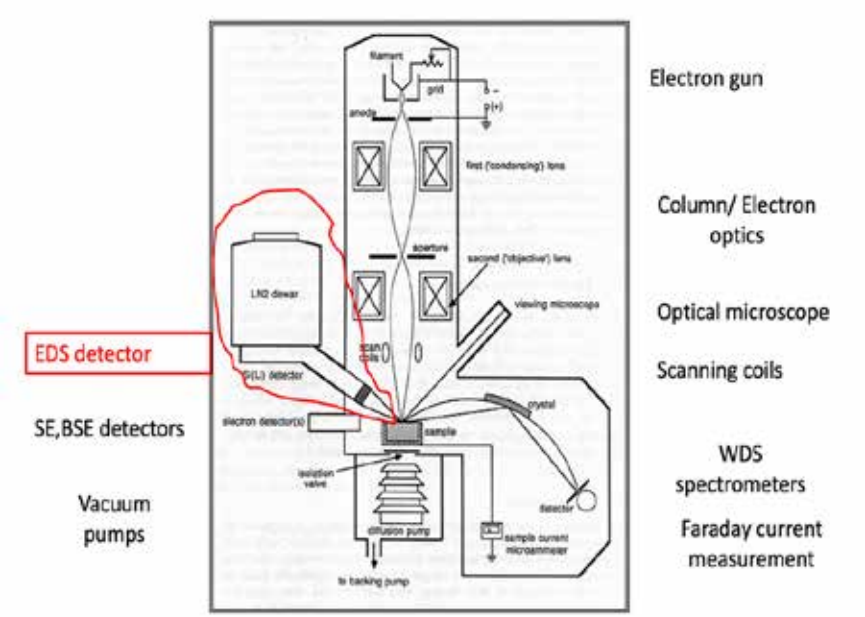

Figure 16. Energy Dispersive Spectroscopy (EDS) location. Source: [27].

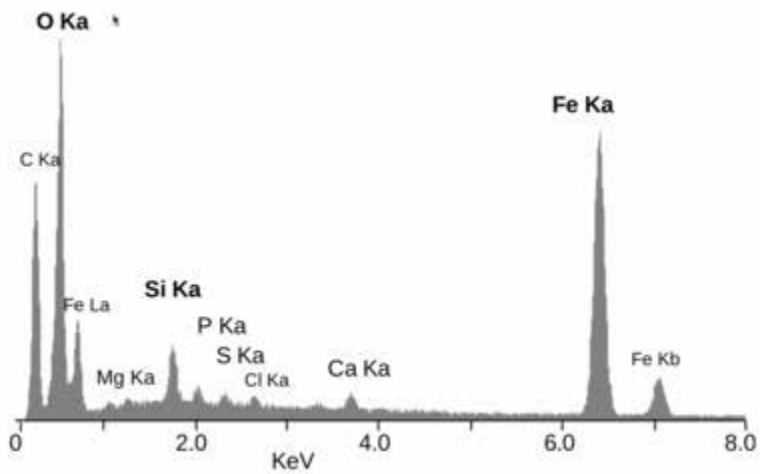

Figure 17. Example of an EDS spectrum. Source: [29].

C. OBJECTIVE

The objectives of this thesis are to measure the material function of heterogenous materials using capillary rheometer to measure the stress components needed and calculate the material functions. We will attempt to calculate the true shear rate and viscosity of non-Newtonian plastic solids and then use the extruded material which is

capable to sustain a true shear and viscosity that can be used for AM. The parts are to be tested and characterized utilizing the different methods mentioned in the previous sections. The objectives of the thesis that are considered could be further broken down into steps:

1. Run tests with the capillary rheometer to quantify the true shear rate and viscosity of the desired non-Newtonian polymer clay to be utilized for 3D printing.
2. Investigate and analyze measured and tabulated true shear rate and viscosity.

Due to the COVID 19 epidemic, the work on the mini rheometers could not be carried out in time for this thesis.

II. EXPERIMENTAL MATERIALS AND METHODS

A. MATERIALS

1. Sculpey Oven Baked Clay

The non-Newtonian material used in this study is original Sculpey oven-baked clay which is a polymer clay and is a plastisol (Figure 18). Sculpey is composed of polyvinyl chloride particles (PVC), augmented with additive materials, plasticizers, and colorants [30]. According to Sculpey, the recommended curing temperature is approximately 135°C and curing time between 10 to 25 minutes, contingent on size and thickness [31]. From the technical data sheet, it has a reported density of 1.1-1.35 g/cm^3 and structure of PVC, the primary ingredient of Sculpey clay shown in Figure 19.

Figure 18. Sculpey oven-baked clay. Source: [31].

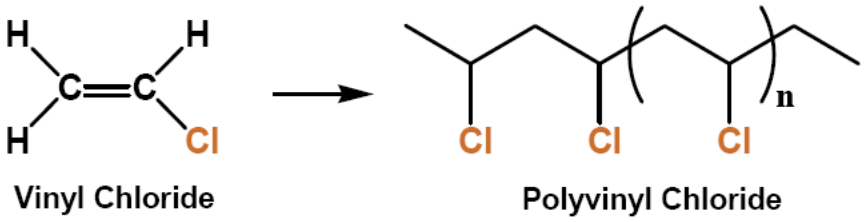

Figure 19. Structure of polyvinyl chloride (PVC). Source: [32].

PVC is a polymer that consists of repeating units (monomers) that are connected (polymerized); in other words, monomers are joined together to form the chains (e.g., building blocks of polymers) to form the chains [33].

B. EQUIPMENT

1. Capillary Rheometer

The capillary rheometer used in this study is ROSAND RH 2000 acquired from Malvern Instruments Ltd [34]. Figure 20 illustrates the components of the capillary rheometer (RH2000). RH 2000 measures the viscosity of a sample of a material by:

- Using a piston inside the bore to force it at a defined speed through a small hole of known size. The hole is in the center of a small metal plug known as capillary die, fitted at the bottom of the bore, and
- Using a pressure transducer to measure the pressure just above the die while
- Controlling the temperature in the bore of the barrel, a tube inside which a piston moves up and down [34].

1-**Crosshead**
2-**Guide rods**
3-**Pressure transducer covers**
4-**Trip reset button**
5-**Control buttons**
6-**Emergency stop button**
7-**Tray**
8-**Force transducer**
9-**Barrel**
10-**Bores**
11-**Piston**
12-**Piston retention collar**
13-**Pressure transducer**

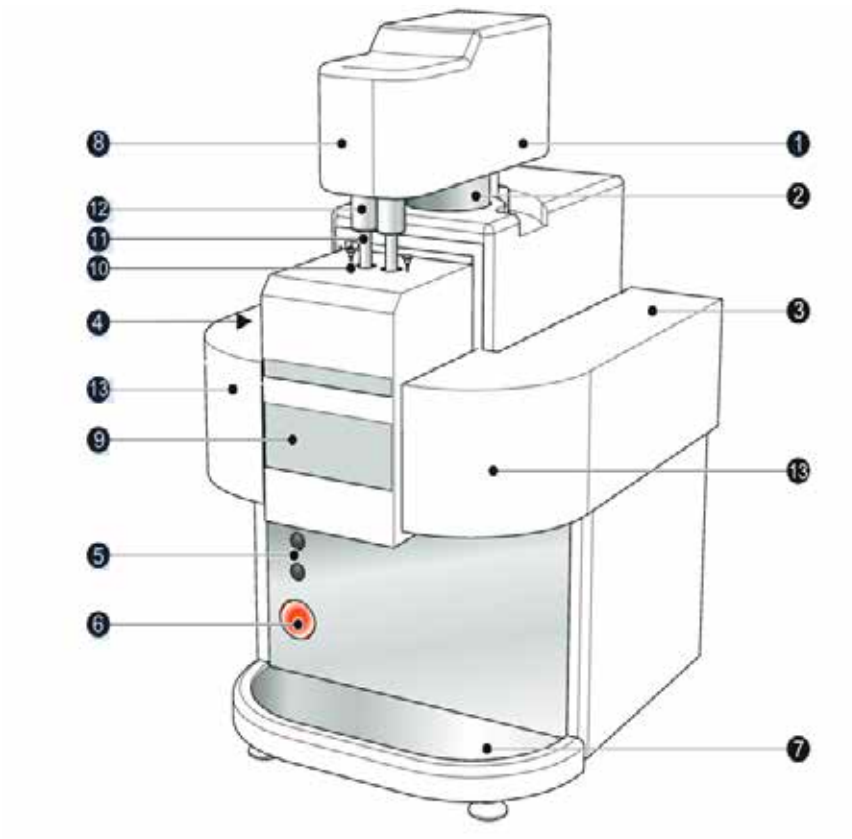

Figure 20. Components of capillary rheometer (RH2000). Source: [34].

The process can be repeated at different speeds to obtain several measurements of viscosity as a function of piston speed or shear rate and at several temperatures to evaluate how the temperature affects viscosity. Rosand RH2000 temperatures range from ambient to 400ºC, with options extending the range to -40ºC to 500ºC. The standard maximum force that can be applied is 12 kilonewton (kN), though a 20kN high force option is available. The viscosity is derived from the pressure measured, the piston speed and the die geometry. The maximum shear rate produce by the rheometer is about 10^7 s^{-1} and the minimum shear rate is 0.1 s^{-1} [34]. The specific system used has twin bores to provide in-situ corrections for non-ideal flow behavior.

2. Mini Rheometer

Mini rheometer is a prototype, not yet tested, that was designed to assist in the experimentation for small scale samples. Figures 21 and 22 illustrate the mini rheometer

prototypes. The intent is to have rheometer with connected cylindrical channels with different radii and lengths. It is constructed with a large diameter top reservoir section for sufficient material feed. Each section would house two transducers to directly measure the pressure drop across each length, so that there is no need for entrance and exit corrections. The transducers considered are piezoelectric rings at transition points and strain gauges attached to the surfaces. These can measure radial expansion, which can be converted to hoop strains and can be calibrated using known pressures to convert the hoop strains to internal pressures. Since the reservoirs are connected, the flow rate is constant for each section. The assembly will secure onto a fixed piece and the material will be pushed from the top with an air pressure or ram. The sizes are as follows: outer diameters (OD) from top to bottom: 19.05 mm, 16 mm, 12 mm, 8.5 mm and 5 mm; and inner diameters (ID) from top to bottom: 12.07 mm, 6 mm, 4 mm and 2 mm. The whole height is about 100 mm. All data taken from the mini rheometer will be theoretically measured and calculated. The theoretical data for the small-scale samples will be compared to the capillary rheometer large scale samples for analogous and/or dissimilar findings. The initial tests with the system showed that the use of piezoelectric rings did not provide sufficient resolution for the pressure measurements, but the strain gauges can provide sufficient pressure resolution and stability. The next iteration will be used to calibrate and measure the pressure differentials.

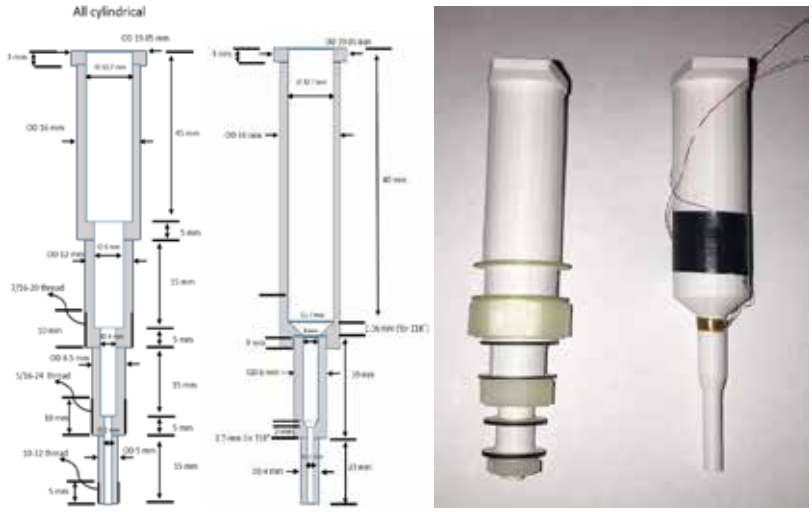

Figure 21. Mini rheometers V1 and V2 designs and 3D printed prototypes

C. SAMPLE PREPARATION

1. Sample Preparation

Sculpey oven-baked clay stored at room temperature prior to be loaded into the RH 2000 capillary rheometer for analysis. Sample was prepared and cut in pieces of 25 mm in length. Figures 22 illustrates Sculpey clay sample pieces used.

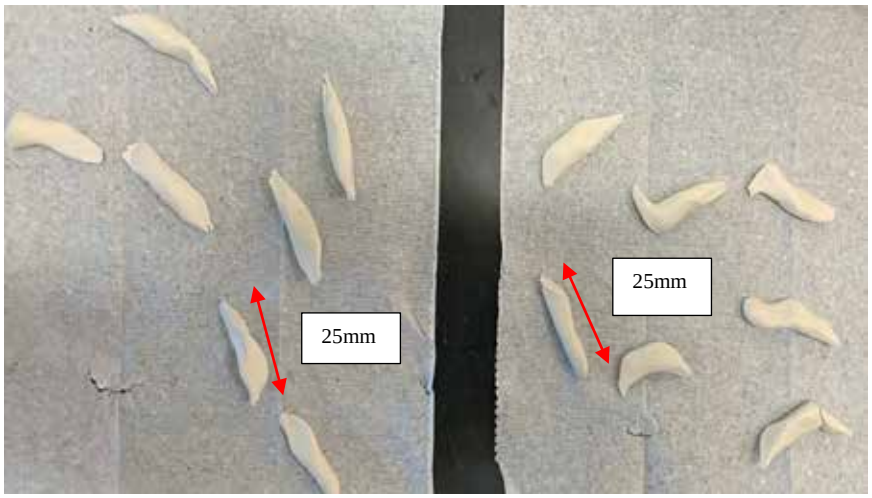

Figure 22. Sculpey clay sample

2. Rosand RH2000 Capillary Rheometer

The capillary rheometer twin bore and piston system is capable of measuring and calculating deformation and flow data used in this study. Figure 23 illustrates Capillary rheometer (i.e. Rosand RH2000). The rheometer was equipped with a 34474 kilopascal (kPa) pressure transducer on the left bore and a 10342 kPa transducer on the right bore to measure pressure right before the inlet of capillary. Three different die orifice diameter and length combinations were utilized (Table 3) and tested using the samples at constant shear rate and shear stress. The data was logged, recorded for the two samples and provided the Bagley and WR corrections.

Figure 23. (Left) Capillary rheometer (Rosand RH2000) (right) Installation of die.

Table 3. Orifice diameter and length of dies

Dies orifice diameter (mm)	Length (mm)
0.5	0.25
0.5	8
1	0.25
1	16
2	0.25
2	32

a. Operation procedures

According to Rosand RH2000 user manual, sample was loaded into the capillary rheometer twin bore system after the operating temperature of 20ºC was reached, and the system was in a steady state and calibrated [34]. Once the respective and selected dies were attached, each bore was loaded with three to four 25 mm piece of the particular sample equivalent 7000 cubic millimeter (mm^3) in volume or 7 cubic centimeter (cc^3) per test. Once the sample was loaded into each bore in turn, each bore was tamped before adding more of the sample in order to reduce the air pockets. It was important to tamp the material in both bores the same way (i.e., applying steady pressure), so that for sensitive samples the conditions in each bore were the same [34]. Before the analysis of each test, the barrels, dies, and pistons were thoroughly cleaned with a cloth and materials provided by the capillary rheometer manufacturer to mitigate product contamination that could impact or interfere with the analysis and the result as well.

b. Testing and data collection

Each test was conducted at sets of constant shear rate to analyze the shear viscosity that is a relationship between the shear rate and shear stress. The test run was

comprised of five stages consisting of a series of constant shear rates [34]. At each stage the test waits for equilibrium, records a result and goes on to the next shear rate in the sequence by increasing the piston speed. The system is designed to provide the Bagley and WR corrections, but the Mooney correction (i.e., wall slip correction) had to be manually calculated and interpolated. For this reason, three different tests were conducted and data collected using the three separate die diameters. Once the test was complete, the data collected produced a shear viscosity versus shear rate graph which were automatically measured and calculated (Figures 31–33 in result section). Viscosity greatly decreased as shear rate increased, showing shear thinning behavior. All different tests are mentioned below.

Tests #1, 2 and 3 were conducted with die diameters and lengths shown in Table 4 in order to measure the shear viscosity, flow properties and rate of deformation of the material used and possibly estimate the thermal stability and wall slip. Figures 24–26 illustrate die used for all three tests.

Table 4. Die sizes used in testing for sample#1

	Bore	Die diameter (mm)	Die length (mm)
Test#1	Left	1	16
	Right	1	0.25
Test#2	Left	2	32
	Right	2	0.25
Test#3	Left	0.5	8
	Right	0.5	0.25

Figure 24. Left and right bore die used for test#1

Figure 25. Left and right bore die used for test#2

Figure 26. Left and right bore die used for test#3

c. Mooney correction

A no-slip condition is often assumed at the wall in the Bagley and WR correction. However, Sculpey exhibits significant wall slip. Thus, the Mooney correction was performed to correct the apparent shear rate utilizing no slip equation to obtain shear rate slip correction. It is important to calculate the true shear rate at the wall to obtain the viscosity in a situation where slip is occurring. Mooney correction requires the measurement by capillary rheometry of the shear stress as a function of apparent shear rate using different die diameters. The die diameters were in the range of 0.5-2 mm (i.e., 0.5, 1, 2 mm). Mooney correction for the wall slip was conducted using the measured and calculated data (e.g., shear viscosity, pressure) recorded during the different tests. Since the velocity changed with the capillary length to diameter ratio, the correction was also conducted to include the dies length and diameter ratio. M. Rides et al. stated although only two different diameters are necessary to determine wall slip, the use of only two dies does not provide an understanding of the confidence in the data since the fit is a linear one [35]. Figure 27 illustrates an example of the Mooney correction plot to achieve slip corrected shear rate performed for polymer melt*s*. The y-intercept of the graph is the apparent shear rate and the x-intercept is the inverse capillary radius. Each curve represents data at different constant values of wall shear stress. For the lines that are horizontal, no wall slip is deduced, but for the lines with positive slopes, the wall slip occurred and velocity can be tabulated [21]. Thus, to improve the accuracy and the quality of data obtained, more than two different dies should be used to plot the straight line. Such information is invaluable for reliably determining the uncertainties in the wall slip [35]. A graphical representation of the flow curve can be plotted by interpolating several experimental data points.

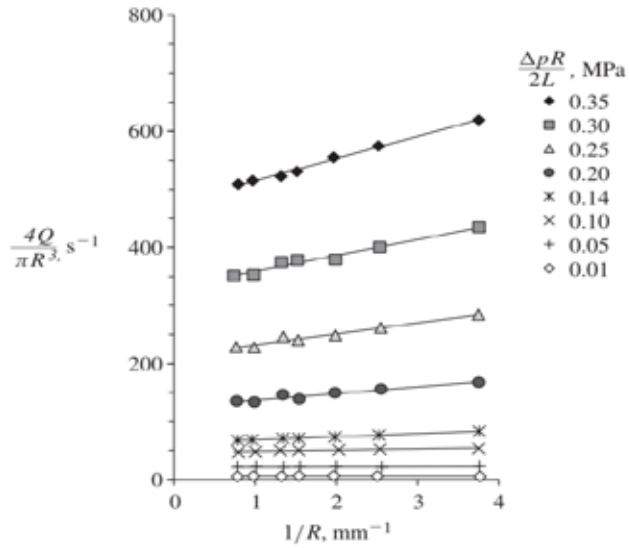

Figure 27. Example of Mooney correction plot. Source [21]

3. Mini Rheometer V1 and V2

Mini rheometers will allow direct measurement of the pressure drop (DP) without the need to correct for entrance exit effects (i.e., Bagley correction). Mass flow rate (Q) will remain the same which can simplify calculations. Only two diameters, one from each mini rheometer, will be used to determine the Mooney correction.

a. Planned operating procedures

A 75-liter air compressor assisted with an air regulator will be utilized to provide sequential pressures at variable times to conduct the calibration and the experiments. For calibration, the air compressor will be connected individually to each mini rheometer (e.g., V1 and V2) with their ends closed. The pressures will be varied using the regulator on the compressor and the strain readings will be recorded for each pressure. These will be used to convert the measured strains into pressure readings.

For the experiments, the rheometers will be filled with Sculpey clay. Once each mini rheometer in turn is filled with the sample, each one will be tamped before adding more of the sample in order to reduce the air pockets. All appropriate safety precautions will be taken due to the pressures going up to 827 kPa. The length of the clay filaments

extruded from each mini rheometer will be measured at different pressure gradients at different time intervals to calculate mass flow rates. Data will be recorded and the previous equations will be used to calculate viscosities. Figure 28 illustrates the 75-liter air compressor assisted with an air regulator that will be used.

Figure 28. 75-liter air compressor assisted with an air regulator used

b. Testing and data collection

All data taken from the mini rheometer will be theoretically measured and calculated. The theoretical data for the small-scale samples will be compared to the capillary rheometer large scale samples for analogous and/or dissimilar findings. The initial tests with the system showed that the use of piezoelectric rings did not provide sufficient resolution for the pressure measurements. The next iteration will involve the use of strain gauges attached to the surface of the sections to measure the hoop strains that will be used to calibrate and measure the pressure differentials. Each test also will be conducted at different pressure gradients at different time intervals and at constant mass flow rate to analyze the shear viscosity that is a relationship between the shear rate and shear stress. Figure 29 illustrates the measurements tool used during this research.

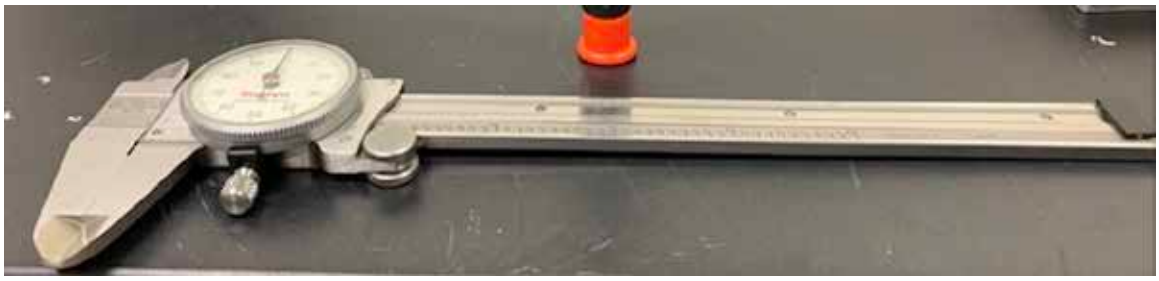

Figure 29. Measurements tool used

c. Mooney correction

For Mooney correction of mini rheometer V1 and V2, the theoretical data will be used to determine the Sculpey clay wall slip rate with a reduced shear rate near the wall. The intention is to take data for the capillaries of different radii and detect areas of shear stress in which high slipping velocities (i.e., speeds) or large changes in the slipping velocity occur. Choosing to operate in the range of high shear stresses or high shear rates can lead to instabilities in the process due to the large changing, or high slipping velocities. Once the Mooney correction is complete, the data will be compared to the data obtained from the capillary rheometer for further analysis.

THIS PAGE INTENTIONALLY LEFT BLANK

III. RESULTS AND DISCUSSION

A. ROSAND RH2000 CAPILLARY RHEOMETER

The pressure drop (DP) versus the diameter was plotted to make sure wall slip was occurring before proceeding with the Mooney correction. Figure 30 illustrates pressure drop versus diameter for polymer clay. If no wall slip occurred, there would be no difference in pressure between the three tested diameters. The cascading effect in pressure change seen as diameter increases indicates wall slip is occurring [36].

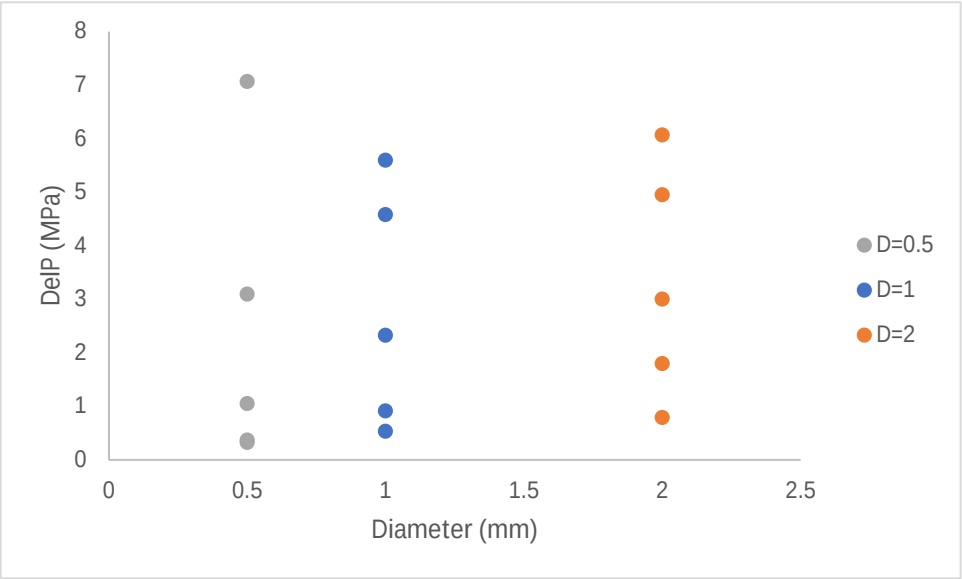

Figure 30. Pressure drop (Dp) versus diameter plot for Sculpey clay.

Since it was determined that wall slip was taking place, Mooney correction was performed. Shear viscosity versus shear rate was plotted for each die for its respective test. Figures 31–33 illustrate shear viscosity versus shear rate plot test#1, 2, and 3 respectively. Viscosity decreased greatly with increasing shear rate which is consistent with this material's behavior. Shear rate is proportional to piston speed and inversely proportional to die radius cubed.

Table 5. Data for test#1(D=1mm)

Shear rate $\gamma(s^{-1})$	Corrected shear rate $\gamma_R(s^{-1})$	Corrected shear stress τ_R (MPa)	Shear viscosity m(Pa.s)	Pressure drop ΔP (MPa)	Flow rate Q mm^3/s	Velocity v (mm/s)
1	1.0701	8.3212	7776.0197	0.5325	$1.1e^{-3}$	$1.4e^{-3}$
3.1622	3.5608	14.2625	4005.3586	0.9128	$3.44e^{-3}$	$4.4e^{-3}$
10	12.0565	36.3501	3014.9602	2.3264	$1.1e^{-2}$	$1.4e^{-2}$
31.6227	41.9961	71.5744	1704.3108	4.5807	$3.44e^{-2}$	$4.4e^{-2}$
100.0487	154.1147	87.4221	567.2534	5.5950	$1.0883e^{-1}$	$1.4e^{-1}$

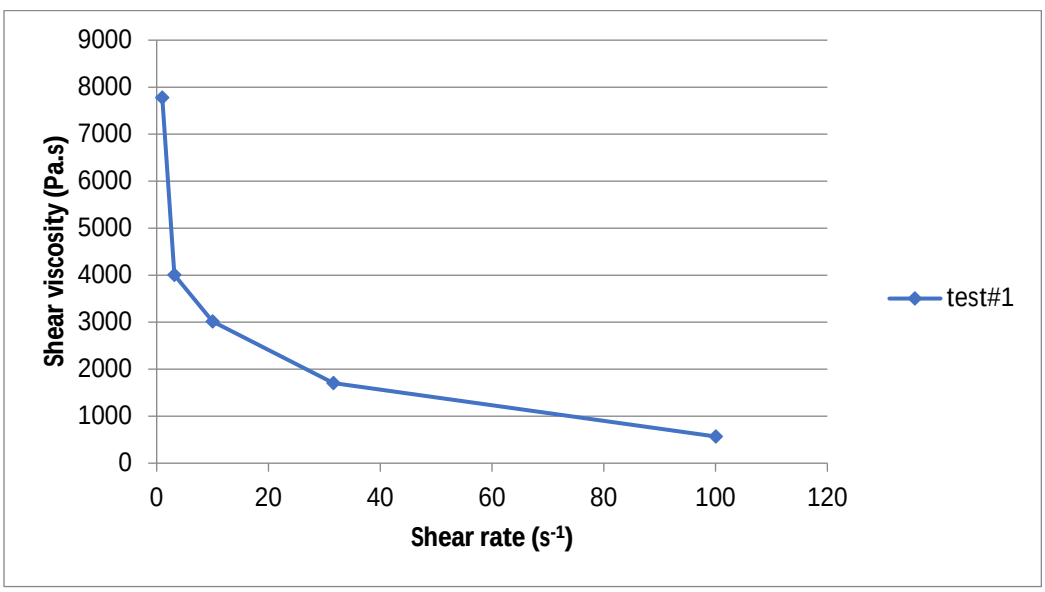

Figure 31. Test#1 viscosity vs. shear rate plot

Table 6. Data for test#2 (D=2mm)

Shear rate $\gamma(s^{-1})$	Corrected shear rate $\gamma_R(s^{-1})$	Corrected shear stress τ_R (MPa)	Shear viscosity m(Pa.s)	Pressure drop ΔP (MPa)	Flow rate Q mm^3/s	Velocity v (mm/s)
1	1.0822	12.3346	11396.8218	0.7894	3.5e-2	$1.11e^{-2}$
3.16227	3.6951	28.0521	7591.5896	1.7953	1.1e-1	$3.5e^{-2}$
10.0084	13.1642	46.8902	3561.9254	3.0009	3.5e-1	$1.11e^{-1}$
31.6150	51.2150	77.3450	1510.2007	4.9500	1.1005	$3.5e^{-1}$
100.0202	264.0128	94.7897	359.0345	6.0665	3.4816	1.1082

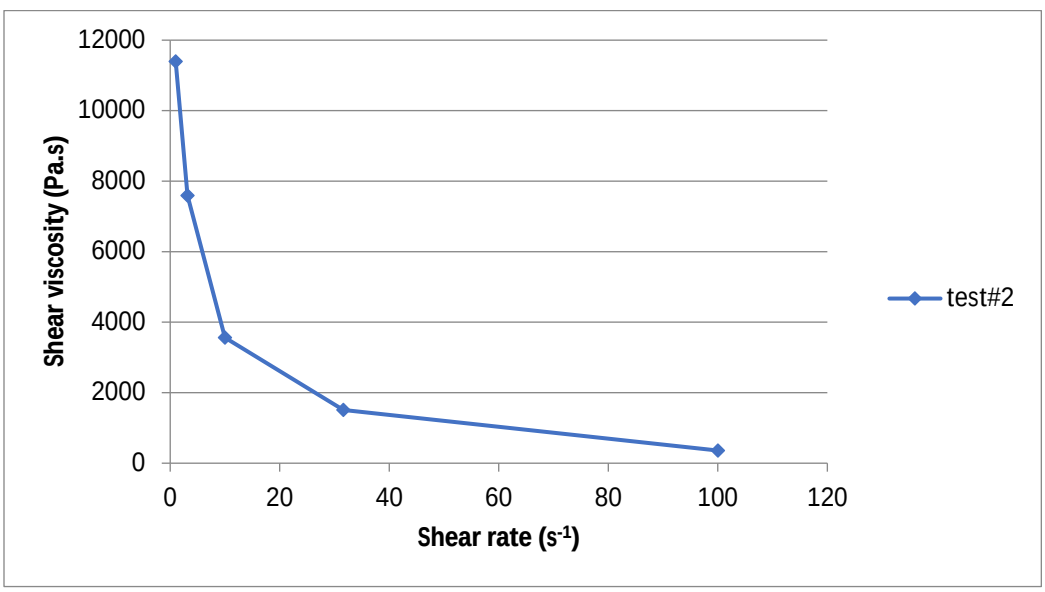

Figure 32. Test#2 shear viscosity vs. shear rate plot

The data for test#3 (0.5 mm diameter) (Figure 33), plot revealed inconsistency and erratic behavior of the polymer possibly due to thermal softening which occurs at these shear rates. The material might be heating as it enters and passes through the very fine (0.5 mm) and long (8 mm) orifice die under the prescribed shear rates. The applied load and piston speed can also cause that effect, pushing too hard and causing instability of the material. Further investigations suggested that the pressure and thermal equilibrium was not achieved within the shear rate steps before moving to the next stage. Unfortunately, this could not be prevented under different equilibrium parameters tested.

Table 7. Data for test#3 (D=0.5mm)

Shear rate $\gamma(s^{-1})$	Corrected shear rate $\gamma_R(s^{-1})$	Corrected shear stress τ_R (MPa)	Shear viscosity m(Pa.s)	Pressure drop ΔP (MPa)	Flow rate Q mm^3/s	Velocity v (mm/s)
1	1.43062	5.0477	3528.3509	0.3230	$3.4e^{-5}$	$1e^{-4}$
3.1622	3.8250	5.7672	1507.7509	0.3691	$1.1e^{-4}$	$5e^{-4}$
10	10.9691	16.3856	1493.7876	1.0486	$3.4e^{-4}$	$1.7e^{-3}$
31.6227	32.5276	48.3235	1485.6154	3.0927	$1.1e^{-3}$	$5.4e^{-3}$
100	98.2783	110.4297	1123.6430	7.0675	$3.4e^{-3}$	$1.731e^{-2}$

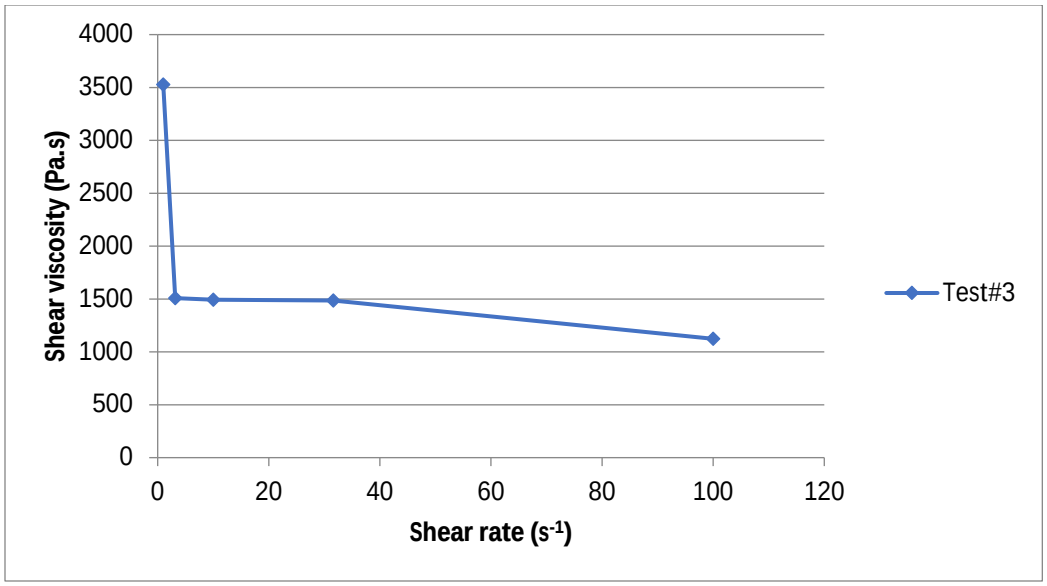

Figure 33. Test#3 shear viscosity vs. shear rate plot

The Sculpey clay viscosity decreases with increasing shear rate. Given that, the capillary rheometer loading with the clay can only operate effectively and provide useful data (e.g., trends) below 2000 Pa; the trend clearly shows an upper bound on one capillary rheometer operating parameter. That is, the minimum shear rate must be between 1 and 0.1 s^{-1}. The down side to this limitation is the high viscosity that is produced which is not adequate for the flow of the materials. Fortunately, the viscosity is so low at planned operating conditions for the clay that viscosity will never be an issue. The data provided a solid baseline to support further research, answer more questions and a step closer to enhance the mechanical and thermal properties of materials, especially for non-Newtonian materials use in AM processing.

Figure 34 illustrates the regression yield plot for each diameter between shear rate and shear stress.

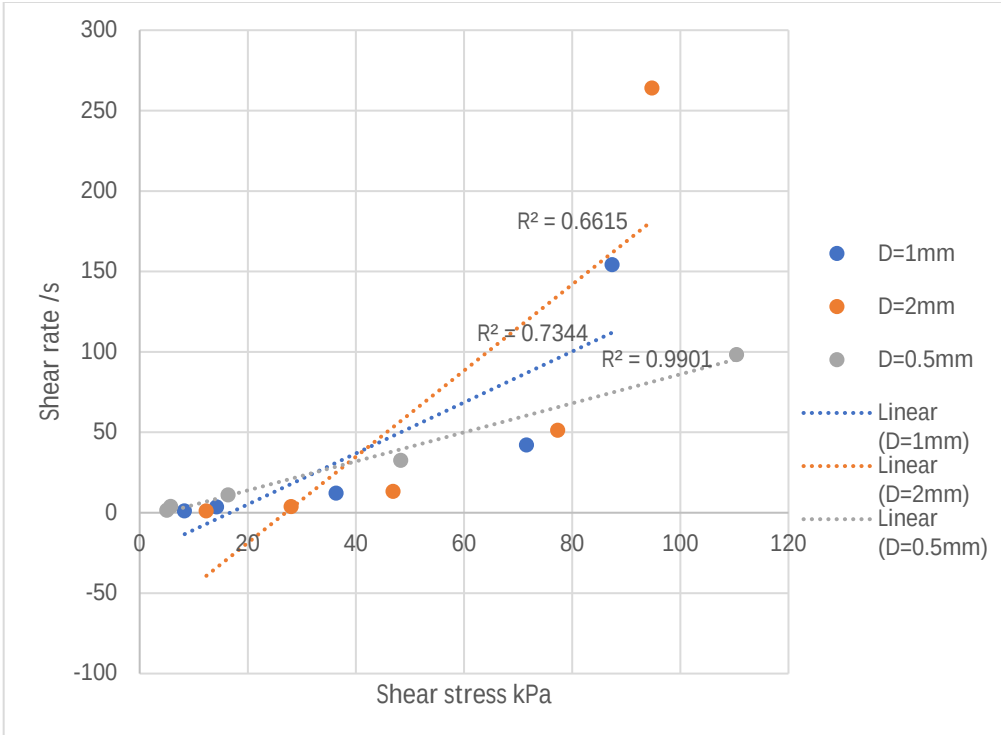

Figure 34. Regression yield plot for each diameter

B. EMPIRICAL MODEL

To determine parameters subject to wall slip is quite challenging and to obtain accurate data requires modeling tools. For this research, to support the Mooney correction and best represent the non-Newtonian plastic behavior of the polymer, the Herschel-Bulkley (HB) with yield stress viscosity model was used. Real fluids are often non-Newtonian fluid, wherein the shear rate exhibited by the materials is related to the shear stress. HB fluid model captures many of the characteristics of real fluids such as yield stress and non-Newtonian behavior. For HB fluids, three factors illustrate this correlation: consistency coefficient (m), flow behavior index (n), and yield stress (t_0) [37].

$$t = t_0 + m\dot{\gamma}^n$$

Figure 35 illustrates the plot of shear stress versus shear rate for test#1, 2 and 3 with power law with yield stress. From the plots, a power law equation and R^2 which was less than 1 were obtained for each test. The fits in general point out that the behavior is

not represented well by HB fluid model, where the shear thinning rate was faster than one given by a power law. This is possibly due to the excessive heating during testing at high shear rates that provides additional softening effect in addition to particle slip and rearrangement in the original polymer clay.

Test#1: t_0 = 8.321248781 kPa t = 8.321248781+8.6616X0.5486

Test#2: t_0 = 12.3346491 kPa t = 12.3346491 +14.883X0.4423

Test#3: t_0 = 5.047747807 kPa t = 5.047747807 +3.6351X0.7206

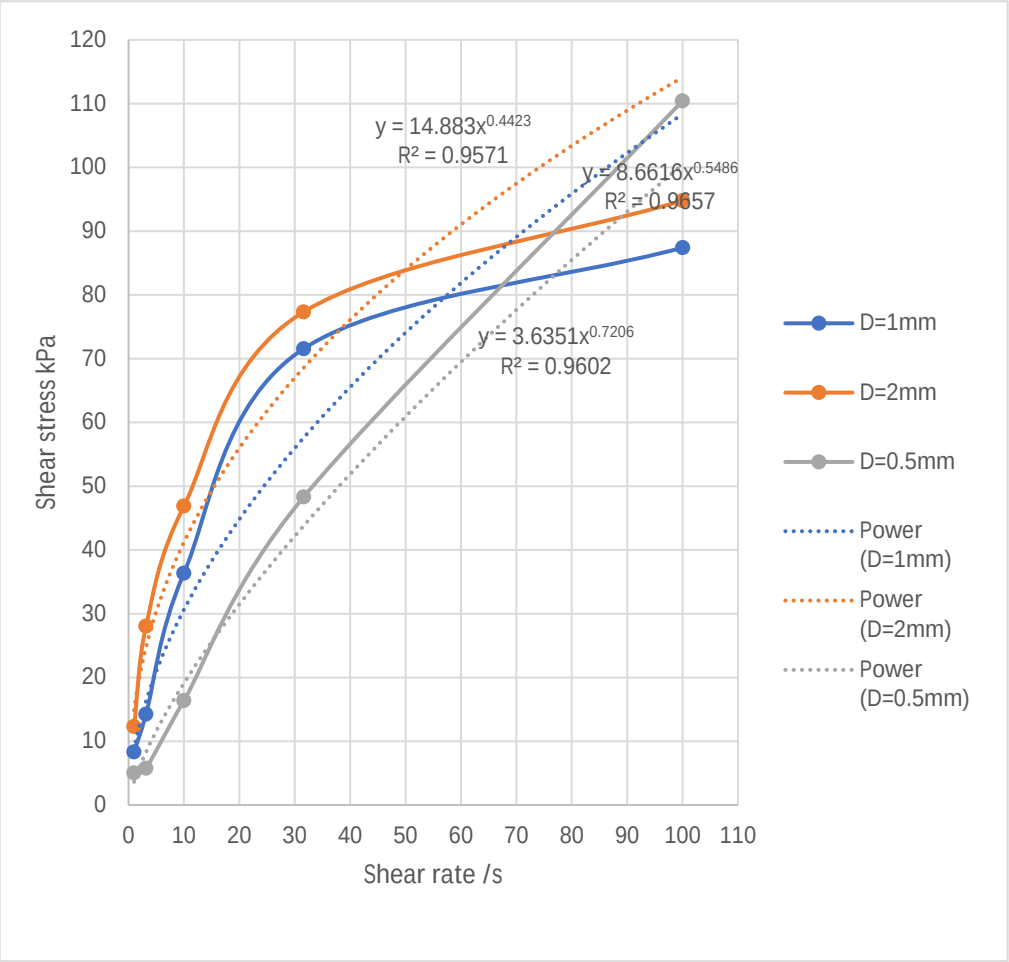

Figure 35. Shear stress vs. shear rate for D = 0.5, 1 and 2 mm using HB model

HB model provide more accurate rheological behavior when adequate experimental data are available and reliable. It also helps identify inconsistency of data due to out of the norm behavior and non-linear errors. Figure 36 illustrates apparent viscosity versus shear rate for each diameter to describe the predicted non-Newtonian behavior.

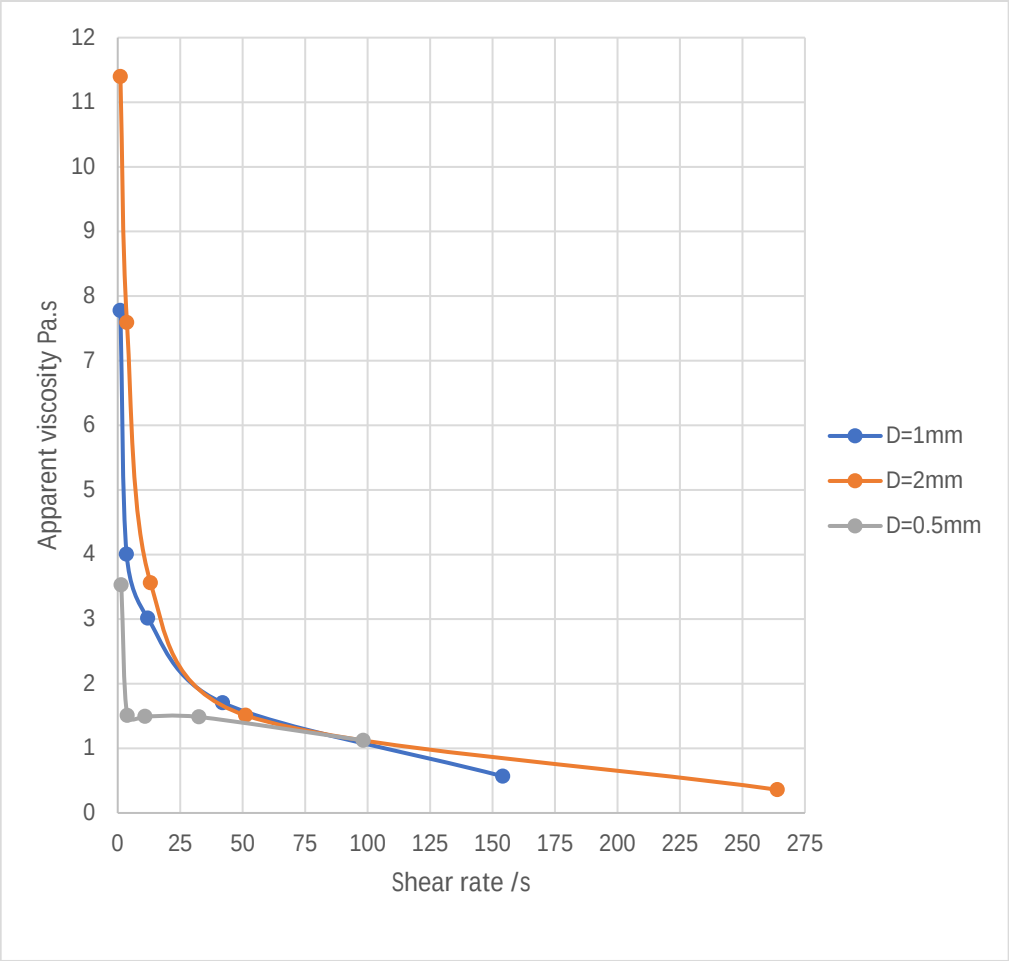

Figure 36. Apparent viscosity vs. shear rate for D = 0.5, 1 and 2 mm using HB model

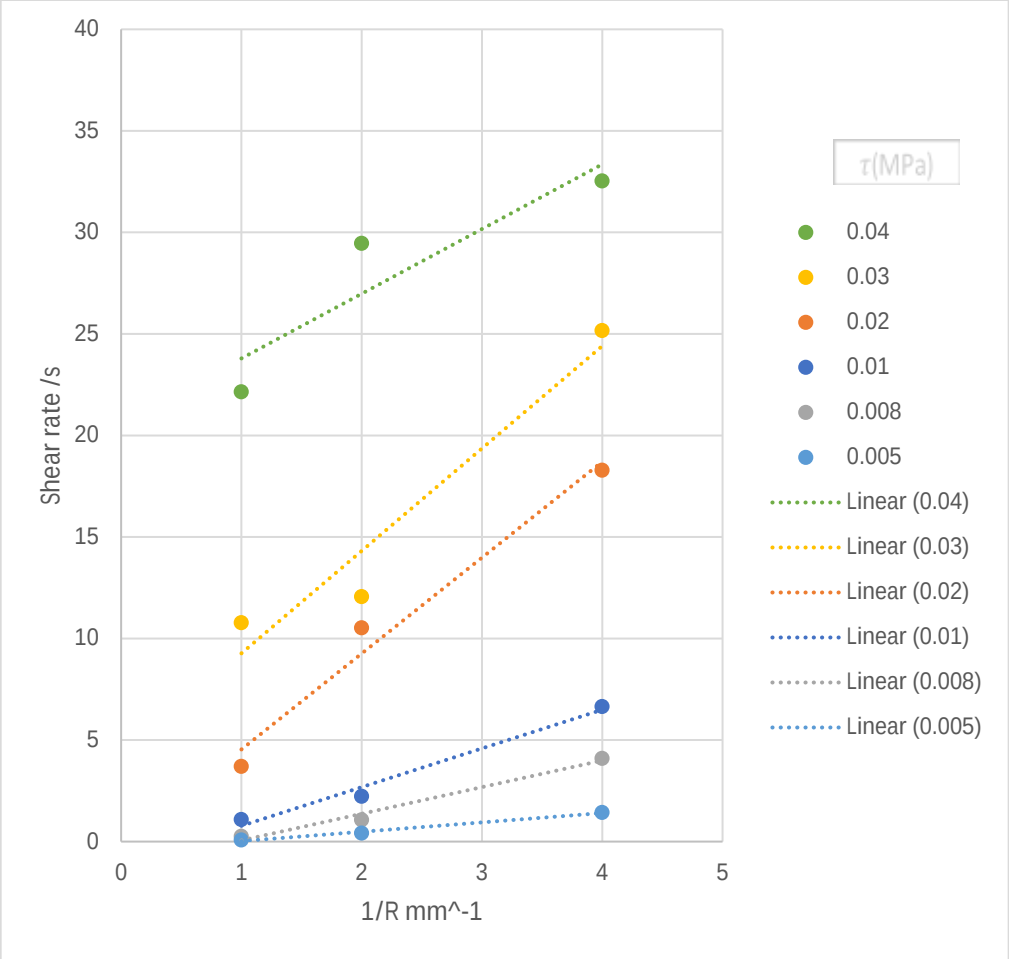

Figure 37. Mooney correction plot

For the measured data, Mooney plots were calculated as shown in Fig. 37. The general trend for all the measurements is that there is significant wall slip, which is proportional to the slope of the curves, within the measurement range. The slopes increase with increasing shear rates and appear to reach nearly constant value beyond a certain shear rate. It is possible that beyond a certain flow rate, the frictional forces reach the yield strength of the material along the walls and the wall slip reaches a constant value.

THIS PAGE INTENTIONALLY LEFT BLANK

IV. CONCLUSION

Additive manufacturing (AM) holds considerable potential in the fabrication of multifunctional composites as well as printing components with optimized three-dimensional (3D) complex geometries layer by layer. However, the mechanical and thermal properties are not optimal for high precision and high-performance applications. For AM applications using powder-based mixtures, it is necessary to understand the rheological properties of these non-Newtonian materials and its effects on deformation, stress, and viscosity, typically measured using a capillary rheometer. This research is focused on the viscosity of non-Newtonian heterogeneous polymer and powder mixtures used for direct-write AM using capillary rheometry and a custom measurement system for small scale testing. The goal was to quantify the viscosity of a non-Newtonian heterogeneous polymer and powder mixture used for direct-write AM.

To achieve this goal, a Rosand dual bore RH2000 capillary rheometer was used and mini rheometer prototypes were designed. In the capillary rheometer, three different tests with a particular die diameter each were conducted. The pressure drop, viscosity and shear rate during the extrusion of a viscous polymer clay were quantified and analyzed. The polymer clay was a commercial plastisol (Sculpey original) that consisted of round polyvinyl chloride particles embedded in a proprietary plasticizer. The die diameters were in the range of 0.5-2 mm (i.e. 0.5, 1, 2mm). The corrections for the entrance/exit and non-Newtonian behavior (i.e., Bagley and WR corrections) were evaluated using the software. Data provided was plotted (shear viscosity versus shear rate) for each die. The analysis of the plots of the first two tests data (i.e., test#1 and 2) where consistent with the material's behavior in which viscosity decreased with increasing shear rate, showing a shear thinning behavior, but test#3 data were inconsistent due to thermal softening which occurs at these shear rates with a very small sized entrance capillary diameter (0.5 mm). Accurate pressure and thermal equilibrium also have to be achieved during the measurements. Despite the inconsistency of test#3 data, the general trend for all the measurements showed significant wall slip. Mooney correction plots were calculated and the measured data were related to the slope of the curves, within the measurement range.

The slopes appear to be nearly constant beyond a certain shear rate. An empirical model, Herschel-Bulkley (HB) model was paired to the Mooney correction in this research to predict a more accurate rheological behavior of the materials. HB model/Mooney correction pair was successful despite to the inconsistency of test#3 data and other factors including, but not limited to, softening effect, particle slip and rearrangement in the original polymer clay.

In the mini rheometers V1 and V2, all data taken were planned to be theoretically measured, calculated and compared to the capillary rheometer for large scale samples for further analysis. However, due to the COVID 19 epidemic, the work on the mini rheometers could not be carried out in time for this thesis.

A full understanding of the material being extruded suitable for 3D printing is needed in order to ensure the objectives are met. Errors and/or discrepancies have a large impact on the outcome of the Mooney correction. Therefore, it is necessary to mitigate inconsistency of data due to factors such as softening effects and particle slip by utilizing well defined die diameters.

V. FUTURE WORK

Future work should focus on the building and calibration of the mini rheometer designs for experimentation. These would be run with new material formulations that are suitable for additive manufacturing developed by other research. The measurements for formulations consisting of different fractions of hard powders embedded in softer binders with different viscosities can complement work on their theoretical and computational modeling to predict material behavior under varying conditions. These can help optimize material formulations that would yield the best properties in 3D printed parts.

THIS PAGE INTENTIONALLY LEFT BLANK

LIST OF REFERENCES

[1] E. Gunduz, "Additive manufacturing of propellants using vibration assisted direct-write printing," presented at SERDP-ESTCP symposium at Alexandria, VA, USA, Nov. 29, 2018. [Online]. Available: https://www.serdp-estcp.org/News-and-Events/Conferences-Workshops/2018-Symposium/2018-Symposium-Archive/Session-4C

[2] J. Scott, N. Gupta, C. Weber, S. Newsome, T. Wohlers, and T. Caffrey, "Additive manufacturing: Status and opportunities," IDA, Science and Technology Policy Institute, Washington, DC, USA, 2012. [Online]. Available: https://www.researchgate.net/profile/Justin_Scott4/publication/297711409_Additive_Manufacturing_Status_and_Opportunities/links/59e7872daca272bc423cf9e7/Additive-Manufacturing-Status-and-Opportunities.pdf

[3] H. Prajapati, D. Ravoori, R. Woods, and A. Jain. "Measurement of anisotropic thermal conductivity and inter-layer thermal contact resistance in polymer fused deposition modeling (FDM)," *Additive Manufacturing*, vol. 21, pp. 84–90, May 2018. [Online]. doi: https://doi.org/10.1016/j.addma.2018.02.019

[4] T. Ngo, A. Kashani, G. Imbalzano, K. Nguyen, and D. Hui. "Additive manufacturing (3D printing): A review of materials, methods, applications and challenges," *Composites Part B: Engineering*, vol. 143, pp. 172–96. Jun. 2018. [Online]. doi: https://doi.org/10.1016/j.compositesb.2018.02.012.

[5] J. Martinez-Pastor, P. Franco & J. Franco-Menchon."Optimization of extrusion process of double-base propellants from their rheological properties," *International Journal of Material Forming*, vol. 12, pp. 307–320. May 2018. [Online]. doi: https://doi.org/10.1007/s12289-018-1418-3

[6] The Department of Defense Systems Information Analysis Center, "Additive manufacturing in the Department of Defense (DOD)." June 9, 2020. [Online]. Available: https://www.dsiac.org/resources/articles/additive-manufacturing-in-the-dod/

[7] P. Alexandrea, "United States Congress passes Defense bill including provisions for additive manufacturing," 3D printing news, May 22, 2018. [Online]. Available: https://www.3dnatives.com/en/us-military-congress-bill240820174/

[8] T. Wohlers, T. Caffrey, and R. I. Campbell, *Wohlers Report 2016: 3D Printing and Additive Manufacturing State of the Industry*, 1st ed, Fort Collins, CO, USA, 2016. [Online]. Available: https://wohlersassociates.com/press71.html

[9] Y, Huang, and M. Leu, (2014) NSF "Additive manufacturing workshop report," presented at Gainesville, Univ. of Florida, FL, USA, Jul. 12, 2013. [Online]. Available: http://plaza.ufl.edu/yongh/2013NSFAMWorkshopReport.pdf

[10] Malvern Panalytical, ROSAND RH2000, 2020 [Online]. Available: https://www.malvernpanalytical.com/rheology-announcement

[11] G. Lewis and E. Schlienger, "Practical considerations and capabilities for laser assisted direct metal deposition," *Mater. Des.* Vol. 21, no 4, pp. 417–423, 2000.

[12] ASTM International "Additive manufacturing overview," Accessed 25-Oct-2020. [Online]. Available: https://www.astm.org/industry/additive-manufacturing-overview.html.

[13] "Brief history of 3d printing," MY3DCONCEPTS, June 19, 2020. [Online]. Available: http://my3dconcepts.com/explore/history-of-3d-printing

[14] S. Tofail, E. Koumoulos, A. Bandyopadhyay, S. Bose, L. O'Donoghue , C. Charitidis , "Additive manufacturing: Scientific and technological challenges, market uptake and opportunities," *Materials* vol. 21, no 1, pp. 22–37. Feb. 2018. [Online]. doi: https://doi.org/10.1016/j.mattod.2017.07.001

[15] J. Wang, H. Xie, Z. Weng, T. Senthil, and L. Wu. "A novel approach to improve mechanical properties of parts fabricated by fused deposition modeling." *Materials & Design* vol. 105, pp. 152–59, Apr. 2016. [Online]. doi: https://doi.org/10.1016/j.matdes.2016.05.078

[16] Voxeljet VXC800. Accessed June 19, 2020. [Online]. Available: https://www.aniwaa.com/product/3d-printers/voxeljet-vxc800

[17] Materialise HeartPrint. Accessed June 19, 2020. [Online]. Available: https://www.materialise.com/en/medical/anatomical-models/heartprint-3d-printed-heart-model

[18] I. E. Gunduz, M. S. McClain, and S. F. Son, "Additive manufacturing of ammonium perchlorate composite propellant with high solids loadings," *Proc. of the Combustion Inst.*, vol. 37, no. 3, pp. 3135–3142, 2019.

[19] I. E. Gunduz, M. S. McClain, P. Cattani, G. T.-C. Chiu, J. F. Rhoads, and S. F. Son, "3D printing of extremely viscous materials using ultrasonic vibrations," *Additive Manufacturing*, vol. 22, pp. 98–103, Aug. 2018.

[20] I. E. Gunduz, M. S. McClain, and S. F. Son, “Additive manufacturing of carbon fiber reinforced silicon carbide solid rocket nozzles,” presented at the AIAA Scitech 2019 Forum, San Diego, CA, Jan. 7–11, 2019.

[21] F. Morrison, *Understanding rheology*. New York, NY, USA: Oxford University Press, 2001, ch. 10, pp. 382–397.

[22] Intertek Group, “Rheology of polymers.” Accessed June 19, 2020. [Online]. Available: https://www.intertek.com/polymers/rheology/

[23] J. Duffy, “Controlling suspension rheology: The physical characteristics of dispersed particles have a large impact on overall rheological properties.” Chemical Engineering, vol. 122, no. 1, pp. 34–39. Jan. 2015, p. 34–39.

[24] G. McNally, D. Smyth, and T. McNally, “The use of dual capillary rheometer techniques as an aid to determining optimum processing conditions in multilayer extrusion,” SAE Technical Paper 1999–01-0375, 1999. [Online]. doi: https://doi.org/10.4271/1999-01-0375.

[25] E. Bagley, “End corrections in the capillary flow of polyethylene,” *Journal of Applied Physics*, vol. 28, pp. 624–627, 1957. [Online]. doi: https://doi.org/10.1063/1.1722814

[26] American Society for Testing and Materials (ASTM) Int. “Physical testing standards and mechanical testing standards.” Accessed Jun. 22, 2019. [Online]. Available: https://www.astm.org/Standards/physical-and-mechanical-testing-standards.html

[27] Jeol Ltd, “Scanning electron microscope A to Z.” Accessed June 19, 2020. [Online]. Available: https://www.jeol.co.jp/en/applications/detail/891.html

[28] Material Evaluation and Engineering, “Energy dispersive X-ray spectroscopy.” Accessed June 19, 2020. [Online]. Available: https://www.mee-inc.com/hamm/energy-dispersive-X-ray-spectroscopyeds

[29] “Energy-dispersive X-ray spectroscopy,” *Wikipedia*. Accessed June 19, 2020. [Online]. Available: https://en.wikipedia.org/wiki/Energy-dispersive_X-ray_spectroscopy

[30] Polyform Products Company, *Premo Sculpey Clay*, MSDS for #32334, 2012. [Online]. Available: http://cdn.dickblick.com/msds/DBH_32334XXXX.pdf

[31] Sculpey, “Sculpey polymer clay for sale.” Accessed October 3, 2020. [Online]. Available: https://www.sculpey.com/

[32] "Polyvinyl chloride," *Wikipedia*, Accessed September 28, 2020. [Online]. Available: https://en.wikipedia.org/wiki/Polyvinyl_chloride

[33] M. Meyers, M.A., K. Chawla, *Mechanical behavior of materials.* New York, USA: Cambridge University Press, 2009.

[34] *Rosand Rh2000 User Manual*. Malvern Instruments, Seattle, WA, USA, 2017, pp. 13–87.

[35] M. Rides and C. Allen, "Slip flow measurement by capillary extrusion Rheometry," Measurement Good Practice Guide, no 90, 2006. [Online]. Available: http://eprintspublications.npl.co.uk/id/eprint/3418

[36] M. Rides, C. Allen, D. Fleming, B. Haworth and A. Kelly, "Intercomparison of slip flow velocity measurements of filled polymers by capillary extrusion Rheometry," *Polymer Test*., vol. 27, no 3, pp. 308–320, 2008.

[37] Implementation of the rheology, "About Implementation of the rheology." Accessed October 28, 2020. [Online]. Available: http://hmf.enseeiht.fr/travaux/beiepe/book/export/html/293

INITIAL DISTRIBUTION LIST

1. Defense Technical Information Center
   Ft. Belvoir, Virginia

2. Dudley Knox Library
   Naval Postgraduate School
   Monterey, California